bioRxiv preprint doi: https://doi.org/10.1101/2020.03.12.988246; this version posted May 18, 2020. The copyright holder for this preprint (which was not certified by peer review) is the author/funder, who has granted bioRxiv a license to display the preprint in perpetuity. It is made available under aCC-BY-NC-ND 4.0 International license.

Highly sensitive and full-genome interrogation of SARS-CoV-2 using multiplexed PCR enrichment followed by next-generation sequencing

Chenyu Li[1#], David N. Debruyne[1#], Julia Spencer[1], Vidushi Kapoor[1], Lily Y. Liu[1], Bo Zhou[2], Utsav Pandey[5], Moiz Bootwalla[5], Dejerianne Ostrow[5], Dennis T Maglinte[5], David Ruble[5], Alex Ryutov[5], Lishuang Shen[5], Lucie Lee[1], Rounak Feigelman[1], Grayson Burdon[1], Jeffrey Liu[1], Alejandra Oliva[1], Adam Borcherding[3], Hongdong Tan[3,4], Alexander E. Urban[2], Xiaowu Gai[5], Jennifer Dien Bard[5], Guoying Liu[1], Zhitong Liu[1*]

[1] Paragon Genomics Inc., Hayward, CA 94545 USA

[2] Department of Psychiatry and Behavioral Sciences, Department of Genetics, Stanford University, CA 94305 USA

[3] MGI, BGI-Shenzhen, Shenzhen 518083 China

[4] BGI-Shenzhen, Shenzhen 518083 China

[5] Department of Pathology and Laboratory Medicine, Children's Hospital Los Angeles, Los Angeles, CA 90027

[#] These authors contributed equally to the work.

[*] Corresponding author's email: zhitong@paragongenomics.com

bioRxiv preprint doi: https://doi.org/10.1101/2020.03.12.988246; this version posted May 18, 2020. The copyright holder for this preprint (which was not certified by peer review) is the author/funder, who has granted bioRxiv a license to display the preprint in perpetuity. It is made available under aCC-BY-NC-ND 4.0 International license.

Abstract

Many detection methods have been used or reported for the diagnosis and/or surveillance of COVID-19. Among them, reverse transcription polymerase chain reaction (RT-PCR) is the most commonly used because of its high sensitivity, typically claiming detection of about 5 copies of viruses. However, it has been reported that only 47-59% of the positive cases were identified by some RT-PCR methods, probably due to low viral load, timing of sampling, degradation of virus RNA in the sampling process, or possible mutations spanning the primer binding sites. Therefore, alternative and highly sensitive methods are imperative. With the goal of improving sensitivity and accommodating various application settings, we developed a multiplex-PCR-based method comprised of 343 pairs of specific primers, and demonstrated its efficiency to detect SARS-CoV-2 at low copy numbers. The assay produced clean characteristic target peaks of defined sizes, which allowed for direct identification of positives by electrophoresis. We further amplified the entire SARS-CoV-2 genome from 8 to half a million viral copies purified from 13 COVID-19 positive specimens, and detected mutations through next generation sequencing. Finally, we developed a multiplex-PCR-based metagenomic method in parallel, that required modest sequencing depth for uncovering SARS-CoV-2 mutational diversity and potentially novel or emerging isolates.

bioRxiv preprint doi: https://doi.org/10.1101/2020.03.12.988246; this version posted May 18, 2020. The copyright holder for this preprint (which was not certified by peer review) is the author/funder, who has granted bioRxiv a license to display the preprint in perpetuity. It is made available under aCC-BY-NC-ND 4.0 International license.

Introduction

A variety of methods for detecting SARS-CoV-2 have been reported and discussed[1,2], including RT-PCR, serological testing[3] and reverse transcription-loop-mediated isothermal amplification[4,5]. Currently, RT-PCR is considered the gold standard for diagnosing SARS-CoV-2 infections because of its ease of use and high sensitivity. RT-PCR has been reported to detect SARS-CoV-2 in saliva[6], pharyngeal swab, blood, rectal swab[7], urine, stool[8], and sputum[9]. In laboratory conditions, the RT-PCR methodology has been shown to be capable of detecting 4-8 copies of virus or lower, through amplification of targets in the Orf1ab, E and N viral genes, at 95% confidence intervals[10-12]. However, only about 47-59% of the true positive cases were identified by RT-PCR, and 75% of RT-PCR negative results were actually later found to be positive with other assays, hence mandating repeated testing [8,13-15]. In addition, there is evidence suggesting that heat inactivation of clinical samples causes loss of viral particles, thereby hindering the efficiency of downstream diagnosis[16].

Therefore, it is necessary to develop robust, sensitive, specific and highly quantitative methods for reliable diagnostics[17,18]. The urgency to develop an effective surveillance method that can be easily used in a variety of laboratory settings is underlined by the wide and rapid spreading of SARS-CoV-2[19-21]. In addition, such method should also distinguish SARS-CoV-2 from other respiratory pathogens such as influenza virus, parainfluenza virus, adenovirus, respiratory syncytial virus, rhinovirus, human metapneumovirus, SARS-CoV, etc., as well as *Mycoplasma pneumoniae*, *Chlamydia pneumoniae* and other causes of bacterial pneumonia[22-25]. Furthermore, obtaining full-length viral genome sequence through next generation sequencing (NGS) prove to be essential for the surveillance of SARS-CoV-2's evolution and for the containment of community spread[26-29]. Indeed, SARS-CoV-2 phylogenetic studies through genome sequence analysis have provided better understanding of the transmission origin, time and routes, which has guided policy-making and management procedures[27,28,30-33].

Here, we describe the development of a highly sensitive and robust detection assay incorporating the use of multiplex PCR technology to identify SARS-CoV-2 infections. Theoretically, the multiplex PCR strategy, by simultaneously targeting and amplifying hundreds of targets, has significantly higher sensitivity than RT-PCR and may even detect nucleotide fragments resulting from degraded viral genomes. Multiplex PCR has been shown to be an efficient and low-cost method to detect Hantaan orthohantavirus and *Plasmodium falciparum* infections[34,35], with high coverage (median 99%), specificity (99.8%) and sensitivity. Moreover, this solution can be tailored to simultaneously address multiple questions of interest within various epidemiological settings[35]. Similar to a recently described metagenomic approach for SARS-CoV-2 identification[36], we also establish a user-friendly multiplex-PCR-based metagenomic method that is capable of detecting SARS-CoV-2, and could also be applied for the identification of novel pathogens with a moderate sequencing depth of approximately 1 million reads.

Results

Mathematical model of RT-PCR

Several RT-PCR methods for detecting SARS-CoV-2 have been reported to date[6,10-12]. Among them, two groups reported the detection of 4-5 copies of the virus[10,12]. To investigate the opportunity for further improvement upon the sensitivity of RT-PCR, we built a mathematical model to estimate the limit of detection (LOD) for SARS-CoV-2. The reported RT-PCR amplicon lengths are around 78-158bp, and the SARS-CoV-2 genome is 29,903bp (NC_045512.2). Thus, we chose 100bp amplicon length and 30kb SARS-CoV-2 genome size for mathematical modeling. With the assumption of 99% RT-PCR efficiency[11], we found that RT-PCR assays could only detect 4.8 copies of SARS-CoV-2 at 95% probability (Fig. 1A), which

bioRxiv preprint doi: https://doi.org/10.1101/2020.03.12.988246; this version posted May 18, 2020. The copyright holder for this preprint (which was not certified by peer review) is the author/funder, who has granted bioRxiv a license to display the preprint in perpetuity. It is made available under aCC-BY-NC-ND 4.0 International license.

is consistent with the experimental results previously reported[10]. In this model, the predicted probability of RT-PCR assays to detect one copy of SARS-CoV-2 is only 26% (Supplemental Fig. 1). This finding may explain, at least in part, the reported 47-56% detection rates of SARS-CoV-2 with known positive samples by RT-PCR[8,13]. We further discovered that the LOD appears to be independent of the viral genome size. For genomes of 4 to 100kb, the detection limit remains 4.8 copies at 95% probability.

One way to elevate the sensitivity is to simultaneously target and amplify multiple regions of the viral genome in a multiplex PCR reaction, thereby increasing the frequency of occurrence in the mathematical model. Amplifying multiple targets has the advantage of potentially detecting fragments of degraded viral nucleotide fragments while tolerating genomic variations, thus allowing for the detection of new and ever-evolving viral strains. The amplification efficiency of multiplex PCR is critical for LOD. We estimated that the efficiency of our multiplex PCR technology is about 26% if using Unique Molecular Identifier (UMI)-labeled primers to count the amplified products after NGS sequencing (Supplemental Fig. 2 and Supplemental Table 1). However, the amplification efficiency could be lower, and amplicons would not be equally amplified if the template used is one single strand of cDNA. Thus, more amplicons are potentially required for multiplex PCR to detect limited copies of the virus.

Mathematical model of multiplex-PCR-based detection method

We designed a panel of 172 pairs of multiplex PCR primers in order to increase the sensitivity of detecting SARS-CoV-2 (Fig. 1B). The average amplicon length is 99bp. The amplicons span across the entire SARS-CoV-2 genome with an average 76bp gap (76±10bp) between adjacent amplicons. Since the observed efficiency of multiplex PCR is about 26% in amplifying the four DNA strands of a pair of human chromosomes, we assumed an efficiency of 6% in amplifying the single-strand of a cDNA molecule. In addition, it has already been reported that 79% of variants are recovered when directly amplifying 600 amplicons from a single cell using our technology[37]. Therefore, we assumed that 80% of targeted regions would be amplified successfully. Using the same mathematical model described above, we estimated that our SARS-CoV-2 panel can detect 1.15 copies of the virus at 95% probability (Fig. 1C). Again, the LOD is independent of virus genome size.

We also designed a second pool of 171 multiplex PCR primer pairs. The target regions of these primer pairs overlap with the gaps between target regions of the previous pool of 172 primer pairs (Fig. 1B). Together, these two overlapping pools of primers provide full coverage of the entire viral genome. Most importantly, using both pools in detection would lead to a calculated detection limit of 0.29 copies at 95% probability.

Detecting limited copies of SARS-CoV-2

The workflow was designed so that the multiplex PCR products are further amplified in a secondary PCR, during which sample indexes and NGS sequencing primers are added (Fig. 1D). The PCR products were first analyzed by electrophoresis to visualize potential positives. Since dozens of target regions could be amplified from a single copy of SARS-CoV-2, electrophoresis peaks with a defined distribution of peak sizes were expected. Multiplex PCR could potentially amplify not only SARS-CoV-2, but also other coronaviruses, due to shared sequence similarities despite the fact that we designed primers specific to the SARS-CoV-2 genome to avoid cross amplification. In that context, electrophoresis analysis provides a fast and sensitive indication of infection from at least that family of viruses. For specificity, the generated NGS sequencing library can be interrogated for definitive identification of the specific virus.

bioRxiv preprint doi: https://doi.org/10.1101/2020.03.12.988246; this version posted May 18, 2020. The copyright holder for this preprint (which was not certified by peer review) is the author/funder, who has granted bioRxiv a license to display the preprint in perpetuity. It is made available under aCC-BY-NC-ND 4.0 International license.

Two plasmids, containing the full sequence of the S and N genes of SARS-CoV-2, respectively, were used to validate our multiplex PCR method. A total of 28 targets are expected to be amplified within our 172-amplicon panel. To simulate the use of real clinical samples, these two plasmids were spiked into cDNA generated from human total RNA. The copy number of each plasmid was precisely determined by droplet-based digital PCR (ddPCR) with a QX200 system from Bio-Rad[38]. The two plasmids were diluted from approximately 9,000 copies to below one copy, and were amplified in multiplex PCR reactions. The library peaks of expected sizes were obtained from 8,900 to 2.8 copies of plasmids (Fig. 2A). Quantification of peaks demonstrated a wide dynamic range from 1 to about 1,000 copies of plasmids (Fig. 2B). The yield of the libraries started to saturate when the copy number reached 1,700. It is possible that the saturation point could be even lower when all of the 172 amplicons are amplified from positive clinical COVID-19 samples, and the library peaks could be observed with even fewer viral copies. In contrast, the detected quantities of a single target on S gene by RT-PCR rapidly dropped when using 2.85 copies (Fig. 2B and Supplemental Fig. 3).

Estimated from the mathematical model described above, employing 28 amplicons provides a 16% chance to detect one single copy of the virus. We tested this predicted probability using one copy of plasmid in multiplex PCR reactions. The theoretical calculation gives a 66% probability to sample 1.1 copies, and a 12% chance to detect them based on a multiplex PCR efficiency of 6%. In practice, we experimentally observed a significantly higher 56% probability to detect 1.1 copies (Fig. 2C). These results suggest that the efficiency of multiplex PCR is actually higher than the previously estimated 6% when a single-stranded cDNA molecule is amplified.

When the amplified products were sequenced, we found that the recovered reads were within a range of about 20-fold relative depth with about 1.4 to 2.8 plasmids, and were uniformly distributed across the GC range (Fig. 2D). When detecting down to 1.4 copies of plasmids, only the reads from one amplicon were about 100-fold lower than the average. Approximately 96% of the amplicons were recovered with 14 copies of plasmids, 77% with 2.8 copies, and 37% with 0.6 copies (Fig. 2E).

Detection of SARS-CoV-2 in COVID-19 specimens

The above two pools of primers were used to amplify the full SARS-CoV-2 genomes from a total of 13 nasopharyngeal swab specimens. These specimens were previously diagnosed to be SARS-CoV-2 positive by using RT-PCR. The viral load was found to be from 8 to 675,885 RNA copies/uL (Supplemental Table 2). These 13 viral genomes were successfully amplified and subsequently sequenced on the Illumina MiSeq. We found a correlation between genome coverage and viral copy number, as expected. While about 95% of the genome was covered at 100X for 8 copies of virus, 98-99% of the genomes were covered at 100X for 22 to 675,885 copies of virus at an average sequencing depth of 5,000 reads per amplicon (Fig. 3A). One genome, from the sample with 5,000 estimated viral copies, was covered at 96% for 100X. This coverage was lower than expected, and might have been caused by the poor sample quality resulting from processing or handling the viral RNA or library.

CleanPlex libraries are usually sequenced at about 1,000 paired-end reads while still generating sufficient data for detecting mutations. To confirm SARS-CoV-2 libraries could be sequenced at about 1,000 reads per amplicon, we sub-sampled the data of 5 genomes to 150,000 and 100,000 total reads per library, which were equivalent to 437 and 291 reads per amplicon, respectively. At least 93% of the genome was covered at 100X with 150,000 total reads, and 86% of the genome was covered at 100X with 100,000 total reads. Even at 50,000 total reads per library, at least 58% of the genome was covered at 100X (Fig. 3B). The high coverage was also manifested by the superior uniformity of the number of

bioRxiv preprint doi: https://doi.org/10.1101/2020.03.12.988246; this version posted May 18, 2020. The copyright holder for this preprint (which was not certified by peer review) is the author/funder, who has granted bioRxiv a license to display the preprint in perpetuity. It is made available under aCC-BY-NC-ND 4.0 International license.

amplicons amplified in the multiplex PCR reaction and recovered in the sequencing (Fig. 3C), and by the $\log_{10}$ distance of the number of each amplicon to the mean number of all amplicons in the library (Fig. 3D).

The mutations in the SARS-CoV-2 genome from the 13 specimens were detected by two independently developed algorithms. Only those mutations that were detected by both methods were reported. Assuming all viral particles from a single patient contained identical mutations, mutations with frequencies (%AF) > 60% were considered to be empirically true. The majority of the mutations identified in these 13 SARS-CoV-2 genomes clustered around 7 loci, probably reflecting the collection of these specimens in close communities or the transmission of the virus (Fig. 3E). According to the similarity of these mutations, samples were categorized into three groups. The majority of the mutations in the first group showed >98% mutation frequency. Groups 1 and 2 shared a considerable number of identical mutations, while Group 3 was significantly different, suggesting that the origin of this isolate might be traced back to a distinct lineage (Supplemental Table 3). Of note, all 13 strains contained at least one mutation that has been reported to be associated with SARS-CoV-2 virulence[39]. The D614G mutation (a G-to-A base change at position 23,403 in the reference strain NC_045512.2), which began spreading in Europe in early February, was then transmitted to new geographic regions and became a dominant form[40], was found in 11 of these 13 specimens.

We considered mutations with %AF ≤ 60% as a likely reflection of intra-host heterogeneity[41]. To eliminate noise from PCR amplification and sequencing, only mutations with %AF ≥ 20% were considered. The 20% cutoff was selected based on the mutation profile from sequencing the synthetic SARS-CoV-2 RNA controls from Twist Bioscience. Some true intra-host mutations with %AF < 20% might be missed. Since no UMI was used in the multiplex PCR amplification, intra-host mutations might still be contaminated with noise originating from PCR amplification, even though a 20% cutoff was applied. The occurrence of such noise may be exacerbated by low viral copy inputs in the multiplex PCR, or low read depth per amplicon in sequencing. In groups 1 and 3, where both viral copy numbers and read depth per amplicon were high, only one intra-host mutation per genome was found in some of the specimens. In contrast, group 2 had low copy numbers, and low read depth per amplicon, and the numbers of apparent intra-host mutations were considerably higher (Fig. 3E and Supplemental Table 3). Some of these intra-host mutations occurred at the aforementioned 7 loci, or were found at other loci and were identical among the 4 specimens in group 2, while the remaining ones appeared random. Our findings suggested that these recurring mutations might not be true intra-host mutations. Indeed, it is possible that the low copy number inputs, as well as sequencing depth, caused a reduction in the %AF, and additionally introduced false intra-host mutations. Therefore, copy number and sequencing depth should be cautiously considered when a mutation is found to have low %AF.

Metagenomic method design for novel pathogens

In order to characterize highly mutated viruses that would otherwise not be amplified by the pre-designed primer pairs, and to discover unknown pathogens, we subsequently developed a user-friendly multiplex-PCR-based metagenomic method. In this method, random hexamer-adapters were used to amplify DNA or cDNA targets in a multiplex PCR reaction. The large amounts of non-specific amplification products were removed by using Paragon Genomics' background removal reagent, thus resolving a library suitable for sequencing. For RNA samples, Paragon Genomics' reverse transcription reagents were used to convert RNA into cDNA, resulting in significantly reduced amount of human ribosomal RNA species.

bioRxiv preprint doi: https://doi.org/10.1101/2020.03.12.988246; this version posted May 18, 2020. The copyright holder for this preprint (which was not certified by peer review) is the author/funder, who has granted bioRxiv a license to display the preprint in perpetuity. It is made available under aCC-BY-NC-ND 4.0 International license.

We sequenced a library made with 4,500 copies of N and S gene-containing plasmids spiked into 10 ng of human gDNA, which roughly represents 3,300 haploid genomes. Even though the molar ratios of viral targets and human haploid genomes were comparable, the N and S genes, which encompass about 4kb of targets, were a negligible fraction of the 3 billion base pairs of a human genome. If every region of the human genome were amplified and sequenced at 0.6 million reads per sample, only one read of viral target would be recovered. In fact, our results showed that 16% of the recovered bases, or 13% of the recovered reads, were within the viral N and S genes (Fig. 4A and Supplemental Table 4). 80% of SARS-CoV-2 and 78% of mitochondrial targets were covered (Fig. 4B), and their base coverage was significantly higher than for human targets (Fig. 4C). In contrast, only 0.08% of human chromosomal regions were amplified. Furthermore, the human exonic regions were preferentially amplified (Fig. 4D). This suggested that the random hexamers deselected a large portion of the human genome, while favorably amplifying regions that were more "random" in base composition. Indeed, long gaps and lack of coverage in very large repetitive regions were observed in human chromosomes (Fig. 4E). On the contrary, the gaps in SARS-CoV-2 and mitochondrial regions were significantly shorter (Fig. 4F). We further optimized this method so that 96% of the SARS-CoV-2 genome was recovered (Fig. 4G). The depth of the recovered bases was within a 10-fold range on average. This 10-fold difference in coverage has been routinely observed with our multiplex PCR technology (Supplemental Fig. 4 and Supplemental Table 5). Therefore, increasing sequencing depth alone might not improve the coverage of the targeted regions further.

Discussion

This study provides a highly sensitive and robust multiplex PCR method for the detection of SARS-CoV-2. By amplifying hundreds of targets simultaneously, our multiplex PCR method is more sensitive than RT-PCR, and tolerates the presence of mutations in SARS-CoV-2. For the purpose of diagnosis, only one of two primer pools could be used, or the two pools could be alternatively used in adjacent samples to prevent cross contamination. While the amplification products from positive samples are mainly viral amplicons, low quantities of primer dimers are produced in the negative samples. Therefore, a simple measurement of the dsDNA concentration by fluorometry or spectrophotometry would not be sufficient. High-resolution electrophoresis is required to resolve the length of the amplification products in order to differentiate the target amplicons from the primer-dimers. Alternatively, a low-depth sequencing in the range of 50K reads per sample would provide definitive diagnostic results.

When both primer pools are used, the entire genome of SARS-CoV-2 can be enriched, sequenced and interrogated for the presence of any mutations. We demonstrated that mutations were detected from samples with viral loads ranging from 8 to half a million copies. For accurate sequencing and phylogenetic studies, a high-depth sequencing in the range of 300K reads per sample, along with an input of high viral load (>100 copies), are deemed necessary. We caution the interpretation of intra-host mutations obtained with a low input number of viral particles and in low sequencing depth data.

The current SARS-CoV-2 panel was demonstrated to specifically amplify the entire SARS-CoV-2 genome, and sequencing data obtained from the 13 COVID-19 RT-PCR positive samples clearly differentiate SARS-CoV-2 from other human coronaviruses, such as MERS-CoV, CoV 229E, CoV OC43, CoV NL63, CoV HKU1. 0% of the obtained sequencing reads from each of the 13 samples were aligned to the genome sequence of any of the above viral species. This is in contrast to what was reported for a similar SARS-CoV-2 panel[42]. Such high specificity argues strongly that this panel could be further expanded to include simultaneous detection of other respiratory viruses including influenza virus.

bioRxiv preprint doi: https://doi.org/10.1101/2020.03.12.988246; this version posted May 18, 2020. The copyright holder for this preprint (which was not certified by peer review) is the author/funder, who has granted bioRxiv a license to display the preprint in perpetuity. It is made available under aCC-BY-NC-ND 4.0 International license.

Metagenomic method is a powerful technology that can theoretically detect any sequences in the specimens. However, metagenomic methods usually require very high sequencing depth in order to find the target sequences, and hence are economically prohibitive as a diagnostic assay. To overcome this constraint, we developed a multiplex-PCR-based metagenomic method that achieved >96% coverage of the S and N genes of SARS-CoV-2 in the contest of human gDNA, while only required ~0.6M of total reads per library. This coverage was superior given the recommended 50% threshold of coverage for drafting a genome[43]. The results were obtained with no additional means of host depletion to remove human gDNA and rRNA. The viral bases were 16% of the total recovered bases in the sequencing. Yet it still necessary to verify and validate the detection of SARS-CoV-2 and the other coronaviruses and respiratory viruses by this metagenomic method.

bioRxiv preprint doi: https://doi.org/10.1101/2020.03.12.988246; this version posted May 18, 2020. The copyright holder for this preprint (which was not certified by peer review) is the author/funder, who has granted bioRxiv a license to display the preprint in perpetuity. It is made available under aCC-BY-NC-ND 4.0 International license.

Materials and Methods

Ethics statement.

Clinical SARS-CoV-2 samples were collected at Children's Hospital of Los Angeles. Samples and ancillary clinical and epidemiological data were de-identified before analysis, and are thus considered exempt from human subject regulations, with a waiver of informed consent according to 45 CFR 46.101(b) of the US Department of Health and Human Services. Analysis of the nasopharyngeal swab samples from patients with COVID-19 disease was approved by the Ministry of Health in the US. Patients in the 2020 COVID-19 outbreak from 1 January 2020 to 30 August 2020 provided oral consent for study enrolment and the collection and analysis of their nasopharyngeal swab. Consent was obtained at the homes of patients or in hospital isolation wards by a team that included staff members of Children's Hospital of Los Angeles. SARS-CoV-2 viruses were purified from the clinical samples by using QIAamp Viral RNA Mini Kit (Qiagen, Cat. No. 52906). The preparations were analyzed by real-time RT–PCR testing for the determination of viral titers of SARS-CoV-2 by standard curve analysis. The full genomes of SARS-CoV-2 viruses were amplified by using the CleanPlex SARS-CoV-2 panel (Paragon Genomics, SKU 918011) and sequenced on an Illumina MiSeq at Children's Hospital of Los Angeles.

Materials

The Universal Human Reference RNA was from Agilent Technologies, Inc. (Cat#74000). The plasmids containing either S or N gene of SARS-CoV-2 (pUC-S and pUC-N, respectively) were purchased from Sangon Biotech, Shanghai, China. The PCR primers used in ddPCR and RT-PCR reactions for S gene are 5'-TGTACTTGGACAATCAAAAAGAGTTGAT and 5'-AGGAGCAGTTGTGAAGTTCTTTTC; for N gene are 5'-GGGGAACTTCTCCTGCTAGAAT and 5'-CAGACATTTTGCTCTCAAGCTG, respectively.

Multiplex PCR panel design

Panel design is based on the SARS-CoV-2 sequence NC_045512.2 (https://www.ncbi.nlm.nih.gov/nuccore/NC_045512.2/). In total, 343 primer pairs, distributed into two separate pools, were selected by a proprietary panel design pipeline to cover the whole viral genome except for 92 bases at its ends. Primers were optimized to preferentially amplify the SARS-CoV-2 cDNA versus background human cDNA or genomic DNA. They were also optimized to amplify the covered genome uniformly.

Reverse transcription

50ng of Universal Human Reference RNA was converted into cDNA using random primers and SuperScript IV Reverse Transcriptase, following the supplier recommended method (Thermo Fisher Scientific, Cat# 18090050). After reverse transcription, cDNA was purified with 2.4X volume of magnetic beads, and washed twice with 70% ethanol. Finally, the purified cDNA was dissolved in 1X TE buffer and used per multiplex PCR reaction.

RT-PCR

Plasmids pUC-S and pUC-N, in combination with human cDNA, were used in each reaction. Paragon Genomics' CleanPlex secondary PCR mix was used with 100nM of each PCR primers in 10ul reactions. The PCR thermal cycling protocol used was 95°C for 10min, then 98°C for 15sec, 60°C for 30sec for 45 cycles.

bioRxiv preprint doi: https://doi.org/10.1101/2020.03.12.988246; this version posted May 18, 2020. The copyright holder for this preprint (which was not certified by peer review) is the author/funder, who has granted bioRxiv a license to display the preprint in perpetuity. It is made available under aCC-BY-NC-ND 4.0 International license.

ddPCR

ddPCR was performed on QX200 from Bio-Rad. Plasmids pUC-S and pUC-N at the estimated copy numbers 1 (6 repeats), 2 (3 repeats), and 100 (3 repeats) were tested. In each reaction, the ddPCR thermal cycling protocol used was 95°C for 5min, then 95°C for 30sec, 60°C for 1min with 60 cycles, 4°C for 5min and 90°C for 5min, 4°C hold. The resulting data were analyzed by following the supplier recommended method.

Multiplex PCR

Paragon Genomics' CleanPlex multiplex PCR reagents and protocol were used. Briefly, a 10µl multiplex PCR reaction was made by combining 5X mPCR mix, 10X Pool 1 of the panel, water and viral template cDNA. The reaction was run in a thermal cycler (95°C for 10min, then 98°C for 15sec, 60°C for 5min for 10 cycles), then terminated by the addition of 2µl of stop buffer. The reaction was then purified by 29µl of magnetic beads, followed by a secondary PCR with a pair of primers for 25 cycles. The secondary PCR added sample indexes and sequencing adapters, allowing for sequencing of the resulting products by high throughput sequencing. A final bead purification was performed after the secondary PCR, followed by library interrogation using a Bioanalyzer 2100 instrument with Agilent High Sensitivity DNA Kit (Agilent Technologies, Inc. Part# 5067-4626).

Mathematical Modeling

A cumulative Poisson probability was used to build the mathematical model. In Microsoft Excel, the following function was used:

P = 1 - POISSON.DIST(1, $\boldsymbol{\lambda}$, TRUE)

For multiplex PCR, $\boldsymbol{\lambda} = f \times 80\% \times n \times m$, where f = frequency of target(s) per genome. $f = l/L$, where l = cumulative length of amplicon, L = length of genome. For a panel of 172 amplicons, l = 172 × average length of amplicon. n = number of virus genomes in the sample (n = 1,2,3…); m = amplification efficiency. 80% of targets were assumed to be successfully amplified in multiplex PCR. For RT-PCR, $\boldsymbol{\lambda} = f \times n \times m$. q = number of detected virus genomes. q is used to plot the graph reported in the paper, e.g., the copies of virus against the matching probabilities. For multiplex PCR, $q = n/a$, a = the number of amplicons used in the multiplex PCR. For RT-PCR, $q = n \times f$.

Multiplex-PCR-based metagenomic method

Paragon Genomics' CleanPlex metagenomic reagents and protocol were used. Briefly, a 10µl multiplex PCR reaction was made by combining 5X mPCR mix, 10X random hexamer-adapters, water and the viral template cDNA. The PCR thermal cycling protocol used was 95°C for 10min, then 98°C for 15sec, 25°C for 2min, 60°C for 5min for 10 cycles. The reaction was then terminated by the addition of 2µl of stop buffer, and purified by 29µl of magnetic beads. The resulting solution was treated with 2µl of CleanPlex reagent at 37°C for 10min to remove non-specific amplification products. After a magnetic bead purification, the product was further amplified in a secondary PCR with a pair of primers for 25 cycles to produce the metagenomic library. This metagenomic library was further purified by magnetic beads before sequencing.

High throughput NGS sequencing and data analysis

bioRxiv preprint doi: https://doi.org/10.1101/2020.03.12.988246; this version posted May 18, 2020. The copyright holder for this preprint (which was not certified by peer review) is the author/funder, who has granted bioRxiv a license to display the preprint in perpetuity. It is made available under aCC-BY-NC-ND 4.0 International license.

High throughput NGS sequencing was performed using Illumina iSeq 100, MiSeq and MGI sequencers (DNBSEQ-G400 and its research-grade CoolMPS sequencing kits). Detailed information for the samples sequenced and used in this manuscript can be found in Supplemental Table 4. Raw sequencing data were trimmed for adaptors using cutadapt version 1.14. The sequences obtained were mapped to the SARS-CoV-2 genome (NC_045512.2) with bwa-mem using Sentieon version 201808.01. Duplicate read marking was skipped. Base-quality recalibration, re-alignment of indels and quality metrics was accomplished with Sentieon. The resulting BAM files were then used to calculate depth and coverage metrics using Samtools version 1.3.1. Algorithms developed independently at Children's Hospital of Los Angeles and paragon Genomics were sued to detect the mutations in the genome of SARS-CoV-2.

Data availability

All sequencing data used in this publication are available for downloading at NCBI's Sequence Read Archive (https://www.ncbi.nlm.nih.gov/Traces/study/?acc=PRJNA614546).

bioRxiv preprint doi: https://doi.org/10.1101/2020.03.12.988246; this version posted May 18, 2020. The copyright holder for this preprint (which was not certified by peer review) is the author/funder, who has granted bioRxiv a license to display the preprint in perpetuity. It is made available under aCC-BY-NC-ND 4.0 International license.

References

1 Yu, F., Du, L., Ojcius, D. M., Pan, C. & Jiang, S. Measures for diagnosing and treating infections by a novel coronavirus responsible for a pneumonia outbreak originating in Wuhan, China. *Microbes Infect* **22**, 74-79, doi:10.1016/j.micinf.2020.01.003 (2020).

2 Zhang, N. *et al.* Recent advances in the detection of respiratory virus infection in humans. *J Med Virol* **92**, 408-417, doi:10.1002/jmv.25674 (2020).

3 Zhang, W. *et al.* Molecular and serological investigation of 2019-nCoV infected patients: implication of multiple shedding routes. *Emerg Microbes Infect* **9**, 386-389, doi:10.1080/22221751.2020.1729071 (2020).

4 Lamb, L. E., Bartolone, S. N., Ward, E. & Chancellor, M. B. Rapid Detection of Novel Coronavirus (COVID-19) by Reverse Transcription-Loop-Mediated Isothermal Amplification. *medRxiv*, 2020.2002.2019.20025155, doi:10.1101/2020.02.19.20025155 (2020).

5 Yu, L. *et al.* Rapid colorimetric detection of COVID-19 coronavirus using a reverse tran-scriptional loop-mediated isothermal amplification (RT-LAMP) diagnostic plat-form: iLACO. *medRxiv*, 2020.2002.2020.20025874, doi:10.1101/2020.02.20.20025874 (2020).

6 To, K. K. *et al.* Consistent detection of 2019 novel coronavirus in saliva. *Clin Infect Dis*, doi:10.1093/cid/ciaa149 (2020).

7 Chen, W. *et al.* Detectable 2019-nCoV viral RNA in blood is a strong indicator for the further clinical severity. *Emerg Microbes Infect* **9**, 469-473, doi:10.1080/22221751.2020.1732837 (2020).

8 Xie, C. *et al.* Comparison of different samples for 2019 novel coronavirus detection by nucleic acid amplification tests. *Int J Infect Dis* **93**, 264-267, doi:10.1016/j.ijid.2020.02.050 (2020).

9 Lin, C. *et al.* Comparison of throat swabs and sputum specimens for viral nucleic acid detection in 52 cases of novel coronavirus (SARS-Cov-2) infected pneumonia (COVID-19). *medRxiv*, 2020.2002.2021.20026187, doi:10.1101/2020.02.21.20026187 (2020).

10 Corman, V. M. *et al.* Detection of 2019 novel coronavirus (2019-nCoV) by real-time RT-PCR. *Euro Surveill* **25**, doi:10.2807/1560-7917.ES.2020.25.3.2000045 (2020).

11 Chu, D. K. W. *et al.* Molecular Diagnosis of a Novel Coronavirus (2019-nCoV) Causing an Outbreak of Pneumonia. *Clin Chem* **66**, 549-555, doi:10.1093/clinchem/hvaa029 (2020).

12 Shirato, K. *et al.* Development of Genetic Diagnostic Methods for Novel Coronavirus 2019 (nCoV-2019) in Japan. *Jpn J Infect Dis*, doi:10.7883/yoken.JJID.2020.061 (2020).

13 Ai, T. *et al.* Correlation of Chest CT and RT-PCR Testing in Coronavirus Disease 2019 (COVID-19) in China: A Report of 1014 Cases. *Radiology*, 200642, doi:10.1148/radiol.2020200642 (2020).

14 Xie, X. *et al.* Chest CT for Typical 2019-nCoV Pneumonia: Relationship to Negative RT-PCR Testing. *Radiology*, 200343, doi:10.1148/radiol.2020200343 (2020).

15 Li, Y. Y. *et al.* [Comparison of the clinical characteristics between RNA positive and negative patients clinically diagnosed with 2019 novel coronavirus pneumonia]. *Zhonghua Jie He He Hu Xi Za Zhi* **43**, E023, doi:10.3760/cma.j.cn112147-20200214-00095 (2020).

16 Zhang, Q. & Zhao, Q. 病毒核酸提取前的高温灭活过程显著降低可检出病毒核酸模板量. *chinaXiv:202002.00034V1*, doi:10.12074/202002.00034 (2020).

17 Lo, Y. M. D. & Chiu, R. W. K. Racing Towards the Development of Diagnostics for a Novel Coronavirus (2019-nCoV). *Clin Chem* **66**, 503-504, doi:10.1093/clinchem/hvaa038 (2020).

18 Liu, Y. *et al.* Clinical and biochemical indexes from 2019-nCoV infected patients linked to viral loads and lung injury. *Sci China Life Sci* **63**, 364-374, doi:10.1007/s11427-020-1643-8 (2020).

19 Bernard Stoecklin, S. *et al.* First cases of coronavirus disease 2019 (COVID-19) in France: surveillance, investigations and control measures, January 2020. *Euro Surveill* **25**, doi:10.2807/1560-7917.ES.2020.25.6.2000094 (2020).

bioRxiv preprint doi: https://doi.org/10.1101/2020.03.12.988246; this version posted May 18, 2020. The copyright holder for this preprint (which was not certified by peer review) is the author/funder, who has granted bioRxiv a license to display the preprint in perpetuity. It is made available under aCC-BY-NC-ND 4.0 International license.

20 Thompson, R. N. Novel Coronavirus Outbreak in Wuhan, China, 2020: Intense Surveillance Is Vital for Preventing Sustained Transmission in New Locations. *J Clin Med* **9**, doi:10.3390/jcm9020498 (2020).

21 Reusken, C. *et al.* Laboratory readiness and response for novel coronavirus (2019-nCoV) in expert laboratories in 30 EU/EEA countries, January 2020. *Euro Surveill* **25**, doi:10.2807/1560-7917.ES.2020.25.6.2000082 (2020).

22 Lin, L. & Li, T. S. [Interpretation of "Guidelines for the Diagnosis and Treatment of Novel Coronavirus (2019-nCoV) Infection by the National Health Commission (Trial Version 5)"]. *Zhonghua Yi Xue Za Zhi* **100**, E001, doi:10.3760/cma.j.issn.0376-2491.2020.0001 (2020).

23 Working Group of Novel Coronavirus, P. U. M. C. H. [Diagnosis and clinical management of 2019 novel coronavirus infection: an operational recommendation of Peking Union Medical College Hospital (V2.0)]. *Zhonghua Nei Ke Za Zhi* **59**, 186-188, doi:10.3760/cma.j.issn.0578-1426.2020.03.003 (2020).

24 Cleemput, S. *et al.* Genome Detective Coronavirus Typing Tool for rapid identification and characterization of novel coronavirus genomes. *Bioinformatics*, doi:10.1093/bioinformatics/btaa145 (2020).

25 Shen, K. *et al.* Diagnosis, treatment, and prevention of 2019 novel coronavirus infection in children: experts' consensus statement. *World J Pediatr*, doi:10.1007/s12519-020-00343-7 (2020).

26 Malik, Y. S. *et al.* Emerging novel coronavirus (2019-nCoV)-current scenario, evolutionary perspective based on genome analysis and recent developments. *Vet Q* **40**, 68-76, doi:10.1080/01652176.2020.1727993 (2020).

27 Li, X., Zai, J., Wang, X. & Li, Y. Potential of large "first generation" human-to-human transmission of 2019-nCoV. *J Med Virol* **92**, 448-454, doi:10.1002/jmv.25693 (2020).

28 Li, X. *et al.* Transmission dynamics and evolutionary history of 2019-nCoV. *J Med Virol* **92**, 501-511, doi:10.1002/jmv.25701 (2020).

29 Ji, W., Wang, W., Zhao, X., Zai, J. & Li, X. Cross-species transmission of the newly identified coronavirus 2019-nCoV. *J Med Virol* **92**, 433-440, doi:10.1002/jmv.25682 (2020).

30 Lu, R. *et al.* Genomic characterisation and epidemiology of 2019 novel coronavirus: implications for virus origins and receptor binding. *Lancet* **395**, 565-574, doi:10.1016/S0140-6736(20)30251-8 (2020).

31 Benvenuto, D. *et al.* The 2019-new coronavirus epidemic: Evidence for virus evolution. *J Med Virol* **92**, 455-459, doi:10.1002/jmv.25688 (2020).

32 Benvenuto, D. *et al.* The global spread of 2019-nCoV: a molecular evolutionary analysis. *Pathog Glob Health*, 1-4, doi:10.1080/20477724.2020.1725339 (2020).

33 Giovanetti, M., Benvenuto, D., Angeletti, S. & Ciccozzi, M. The first two cases of 2019-nCoV in Italy: Where they come from? *J Med Virol* **92**, 518-521, doi:10.1002/jmv.25699 (2020).

34 No, J. S. *et al.* Comparison of targeted next-generation sequencing for whole-genome sequencing of Hantaan orthohantavirus in Apodemus agrarius lung tissues. *Sci Rep* **9**, 16631, doi:10.1038/s41598-019-53043-2 (2019).

35 Tessema, S. K. *et al.* Sensitive, highly multiplexed sequencing of microhaplotypes from the *Plasmodium falciparum* heterozygome. *bioRxiv*, 2020.2002.2025.964536, doi:10.1101/2020.02.25.964536 (2020).

36 Chen, L. *et al.* RNA based mNGS approach identifies a novel human coronavirus from two individual pneumonia cases in 2019 Wuhan outbreak. *Emerg Microbes Infect* **9**, 313-319, doi:10.1080/22221751.2020.1725399 (2020).

bioRxiv preprint doi: https://doi.org/10.1101/2020.03.12.988246; this version posted May 18, 2020. The copyright holder for this preprint (which was not certified by peer review) is the author/funder, who has granted bioRxiv a license to display the preprint in perpetuity. It is made available under aCC-BY-NC-ND 4.0 International license.

37 Ericson, N. G. *et al.* Abstract 439: Targeted single cell DNA sequencing without prior whole genome amplification for mutational analysis of circulating tumor cells. *Cancer Research* **79**, 439-439, doi:10.1158/1538-7445.Am2019-439 (2019).

38 Dong, L. *et al.* Comparison of four digital PCR platforms for accurate quantification of DNA copy number of a certified plasmid DNA reference material. *Sci Rep* **5**, 13174, doi:10.1038/srep13174 (2015).

39 Yao, H. *et al.* Patient-derived mutations impact pathogenicity of SARS-CoV-2. *medRxiv*, 2020.2004.2014.20060160, doi:10.1101/2020.04.14.20060160 (2020).

40 Korber, B. *et al.* Spike mutation pipeline reveals the emergence of a more transmissible form of SARS-CoV-2. *bioRxiv*, 2020.2004.2029.069054, doi:10.1101/2020.04.29.069054 (2020).

41 Ramazzotti, D. *et al.* Characterization of intra-host SARS-CoV-2 variants improves phylogenomic reconstruction and may reveal functionally convergent mutations. *bioRxiv*, 2020.2004.2022.044404, doi:10.1101/2020.04.22.044404 (2020).

42 St Hilaire, B. G. *et al.* A rapid, low cost, and highly sensitive SARS-CoV-2 diagnostic based on whole genome sequencing. *bioRxiv*, 2020.2004.2025.061499, doi:10.1101/2020.04.25.061499 (2020).

43 Ladner, J. T. *et al.* Standards for sequencing viral genomes in the era of high-throughput sequencing. *mBio* **5**, e01360-01314, doi:10.1128/mBio.01360-14 (2014).

bioRxiv preprint doi: https://doi.org/10.1101/2020.03.12.988246; this version posted May 18, 2020. The copyright holder for this preprint (which was not certified by peer review) is the author/funder, who has granted bioRxiv a license to display the preprint in perpetuity. It is made available under aCC-BY-NC-ND 4.0 International license.

Acknowledgements

The authors would like to thank Jian Xu of MGI, BGI-Shenzhen for technical support in MGI sequencing, Dr. Jin Billy Li of Stanford University for the coordination of academic support, Dr. Alexander E. Urban of Stanford University for suggestions in preparing the manuscript, and Dr. Zihuai He of Stanford University for discussions on a potential mathematical model of the metagenomic method.

Author contributions

C.L., D.N.D., Z.L. conceived the study and drafted the manuscript. C.L., D.N.D., J.S., V.K., L.Y.L., L.L., R.F., G.B., J.L., A.O., G.L., Z.L. performed experiments, analysis and revised the manuscript. U. P. performed the initial diagnosis and quantification of clinical COVID-19 samples. D. O and D. R. performed CleanPlex library preparation and NGS sequencing of the positive COVID-19 clinical samples with MiSeq. M. B., D. M., A. R., and L. S. analyzed the data from the clinical samples. X. G. and J. D. B. supervised the study of clinical samples and revised the manuscript. B.Z., A.E.U. performed ddPCR experiments and analysis. A.B., H.T. performed MGI sequencing and analysis.

Conflict of Interest

The authors declare no competing interests.

bioRxiv preprint doi: https://doi.org/10.1101/2020.03.12.988246; this version posted May 18, 2020. The copyright holder for this preprint (which was not certified by peer review) is the author/funder, who has granted bioRxiv a license to display the preprint in perpetuity. It is made available under aCC-BY-NC-ND 4.0 International license.

Figure 1. Mathematical model, primer design and workflow

(**A**) A mathematical model of RT-PCR based on Poisson process. The LOD is 4.8 copies of virus at 95% probability. (**B**) Two overlapping pools of multiplex PCR primers, shown on the right of the genome of SARS-CoV-2, were designed to span the entire viral genome. Pool 1, containing 172 pairs of primers, covers 56.9% of the viral genome and was used in the detection. Pool 2 contains 171 pairs of primers and covers 56.4% of the genome. Both pools are used to cover the full length of the genome. (**C**) A mathematical model of multiplex PCR with pool 1 of the primers. The LOD is 1.15 copies of virus at 95% probability. (**D**) The workflow of the multiplex PCR method. The prepared libraries can be detected using high-resolution electrophoresis, and sequenced together with other samples using high-throughput sequencing.

Figure 2. Detection of SARS-CoV-2 gene-containing plasmids by electrophoresis and sequencing

(**A**) Two plasmids, containing SARS-CoV-2 S and N genes, respectively, were diluted in human cDNA and amplified in multiplex PCR with pool 1 (172 pairs of primers). The number of plasmid copies per reaction, determined by ddPCR, were from 8,900 to 0.6. The resulting products obtained after multiplex PCR were resolved by electrophoresis. The specific amplification products (the library) can still be seen with 2.8 copies of plasmids. (**B**) The library yields can be detected down to 0.6 copies of plasmids (n=4) by multiplex PCR (black line), while only down to 2.8 copies by RT-PCR (> 4.5-fold difference) (red line). (**C**) Poisson process was used to estimate the chance of sampling around 1 copy of viral particles, and the mathematical model was used to estimate the chance of detecting them (red line). There is 12% of probability to detect 1.1 copies with a multiplex PCR efficiency of 6%. In reality, we observed a significantly higher 56% probability for 1.1 copies and 100% probability for 1.4 copies. (**D**) After sequencing 1.4 and 2.8 copies of plasmids, the reads of all 28 amplicons spanning both N and S genes were clustered within a 20-fold range of coverage (n=3). With 1.4 copies, only the reads of one amplicon were about 100-fold lower than the average (n=3). (**E**) About 96% of amplicons were recovered with 14 copies of plasmids, 77% with 2.8 copies, and 37% with 0.6 copies (n=3).

Figure 3. Sequencing the whole genome of SARS-CoV-2 in COVID-19 positive samples

(**A**). The entire genomes of SARS-CoV-2 were amplified and sequenced from a cohort of 13 COVID-19 positive patients. The copies of virus that were used in the multiplex PCR reaction range from 8 to 675,885. 98.3-99.9% of the genomes were covered at 100X with an average of 5,000 reads per amplicon from 22 to 675,885 copies. The coverage slightly decreased to 95% with 8 copies of virus. (**B**) Sub-sampling of 5 samples to 150,000 total reads slightly reduced the 100X coverage to 93-97%. (**C**) The amplification performance of the 343 amplicons for each sample was measured by the uniformity of 0.2X mean of the reads. Each circle represents one sample. (**D**) In one sample, the performance of each amplicon was evaluated by their $\log_{10}$ distance to the mean reads. Each circle represents one amplicon. (**E**). The mutations in each SARS-CoV-2 genome were detected and the SARS-CoV-2 samples were segregated into 3 groups based on similarities. The majority of the mutations were shared by groups 1 and 2. Group 2 contained low viral copy numbers in multiplex PCR, low reads per amplicon in sequencing and a considerable amount of apparent intra-host mutations. Mutations in group 3 were different from the other 2 groups. The mutations that associate with virulence[39] are in bold. A23403G, which associates with high transmission[40], is in red. The reference genome used was NC_045512.2. Black vertical lines represent point mutations, green vertical lines represent intra-host mutations, red vertical lines represent deletions.

bioRxiv preprint doi: https://doi.org/10.1101/2020.03.12.988246; this version posted May 18, 2020. The copyright holder for this preprint (which was not certified by peer review) is the author/funder, who has granted bioRxiv a license to display the preprint in perpetuity. It is made available under aCC-BY-NC-ND 4.0 International license.

Figure 4. Multiplex PCR-based metagenomic method for the detection of SARS-CoV-2 genes

(**A**) Random hexamer-adapters were used in multiplex PCR to amplify 4,500 copies of plasmids in the background of 3,300 haploid human gDNA molecules. The resulting libraries were sequenced at an average of 0.6 million total reads. Of the total bases recovered, 16% were mapped to SARS-CoV-2 S and N genes. (**B**) 80% of S and N genes, and 78% of the human mitochondrial chromosome were amplified with >= 1X coverage, while only 0.08% of the human chromosomes were. (**C**) On average, S and N genes were covered at 2,346X, mitochondrial and human chromosomes at 77X and 20X, respectively. (**D**) Human exons were relatively over-amplified, at about 4-fold higher compared to their actual ratio within the genome. (**E**) Gaps and long regions of absence of amplification were observed for human chromosomes. An example shown here is chromosome Y. Small gaps were additionally found in the enlarged cluster of amplification. The long absent region (red double arrow) overlapped with the repetitive regions on Y chromosome. (**F**) Representation of the recovered regions in S and N genes and the human mitochondrial chromosome. The coverage was from 1,000- to 10,000-fold for S and N genes, and 30- to 500-fold for the mitochondrial chromosome. (**G**) This metagenomic method was subsequently improved, resulting in 95.7% of the SARS-CoV-2 S gene covered at 22.5X and 96.2% of the N gene covered at 12.8X, with a sequencing depth of 0.53M total reads.

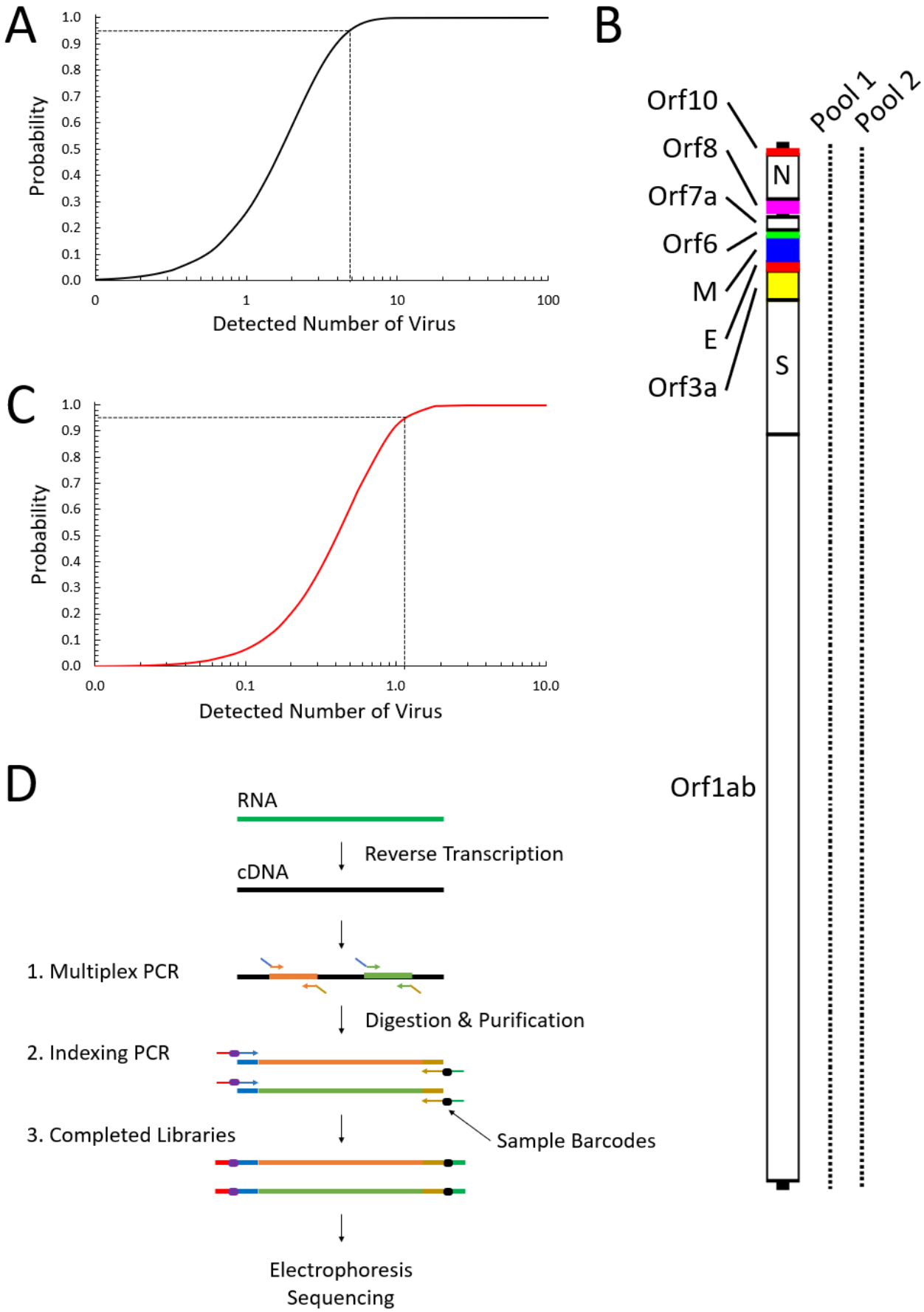
A
Probability
1.0
0.9
0.8
0.7
0.6
0.5
0.4
0.3
0.2
0.1
0.0
0
1
10
100
Detected Number of Virus
B
Orf10
Orf8
Orf7a
Orf6
M
E
Orf3a
N
S
Orf1ab
Pool 1
Pool 2
C
Probability
0.0
0.1
1.0
10.0
Detected Number of Virus
D
RNA
Reverse Transcription
cDNA
1. Multiplex PCR
Digestion & Purification
2. Indexing PCR
3. Completed Libraries
Sample Barcodes
Electrophoresis
Sequencing

Figure 1

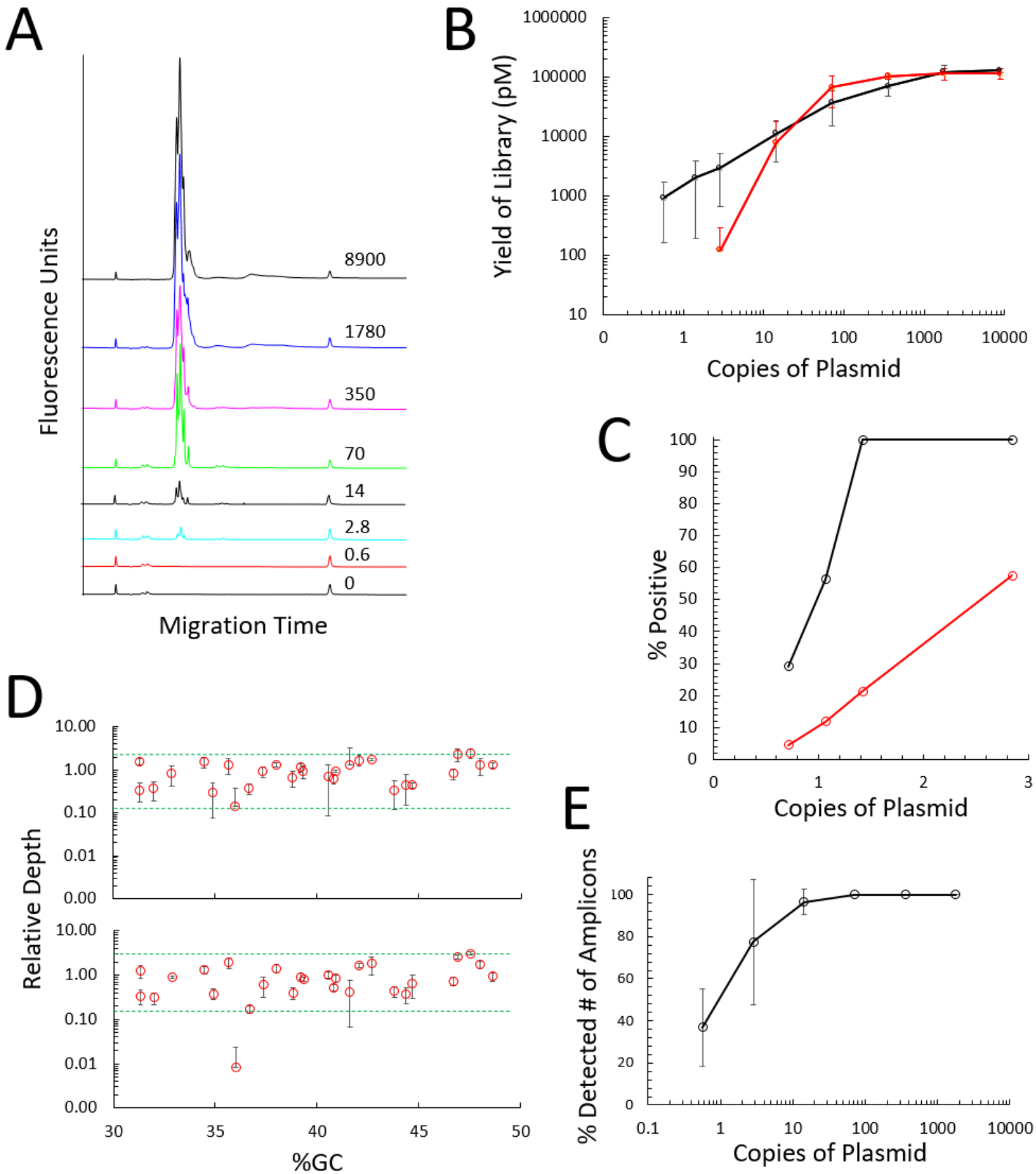
A
Fluorescence Units
8900
1780
350
70
14
2.8
0.6
0
Migration Time
B
Yield of Library (pM)
1000000
100000
10000
1000
100
10
0
1
10
100
1000
10000
Copies of Plasmid
C
% Positive
100
90
80
70
60
50
40
30
20
10
0
0
1
2
3
Copies of Plasmid
D
Relative Depth
10.00
1.00
0.10
0.01
0.00
30
35
40
45
50
%GC
E
% Detected # of Amplicons
100
80
60
40
20
0
0.1
1
10
100
1000
10000
Copies of Plasmid

Figure 2

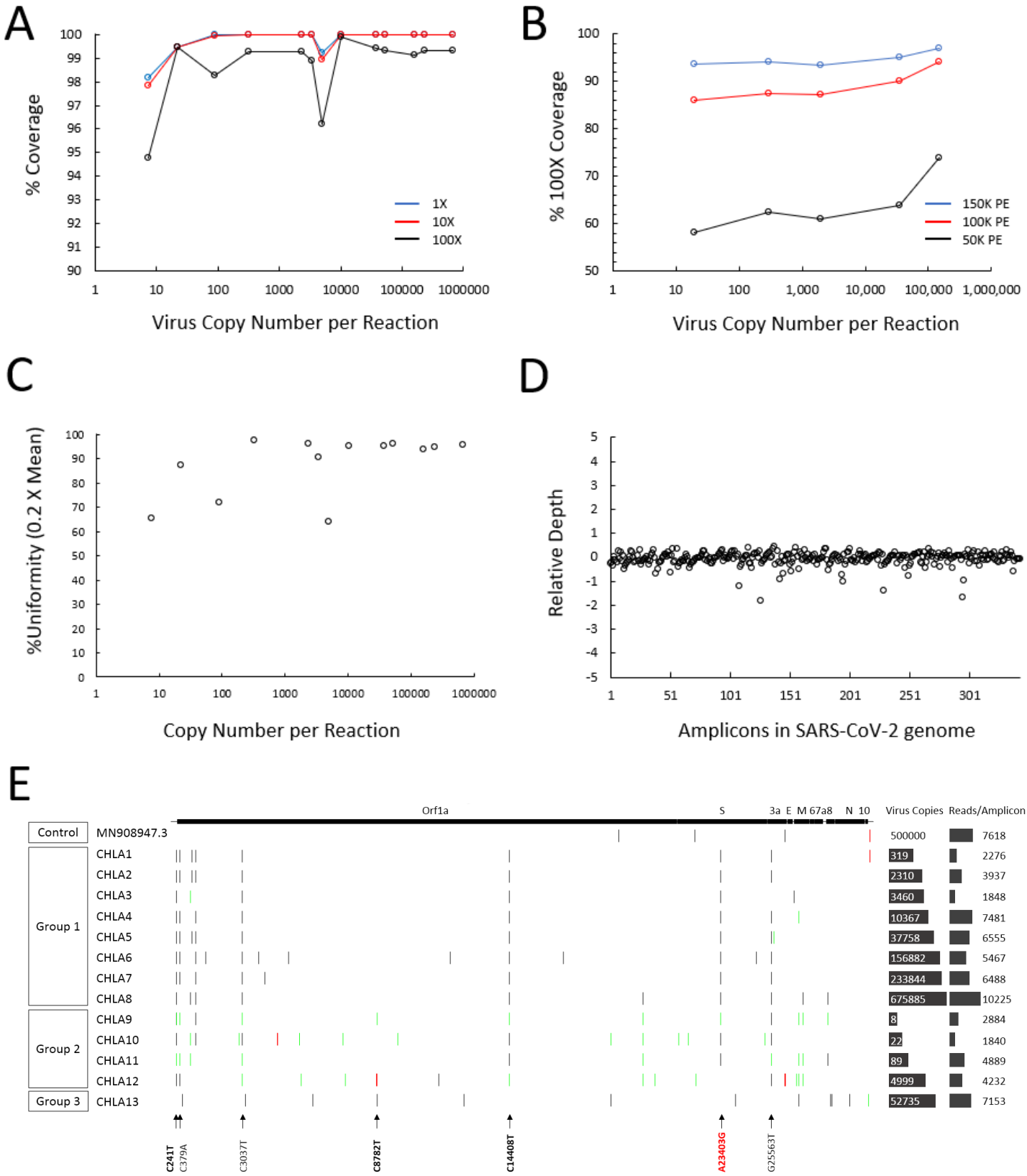
A
% Coverage
Virus Copy Number per Reaction
1X
10X
100X
B
% 100X Coverage
Virus Copy Number per Reaction
150K PE
100K PE
50K PE
C
%Uniformity (0.2 X Mean)
Copy Number per Reaction
D
Relative Depth
Amplicons in SARS-CoV-2 genome
E
Orf1a
S
3a E M 67a8 N 10
Virus Copies
Reads/Amplicon
Control
MN908947.3
Group 1
CHLA1
CHLA2
CHLA3
CHLA4
CHLA5
CHLA6
CHLA7
CHLA8
Group 2
CHLA9
CHLA10
CHLA11
CHLA12
Group 3
CHLA13
500000 7618
319 2276
2310 3937
3460 1848
10367 7481
37758 6555
156882 5467
233844 6488
675885 10225
8 2884
22 1840
89 4889
4999 4232
52735 7153
C241T
C379A
C3037T
C8782T
C14408T
A23403G
G25563T

Figure 3

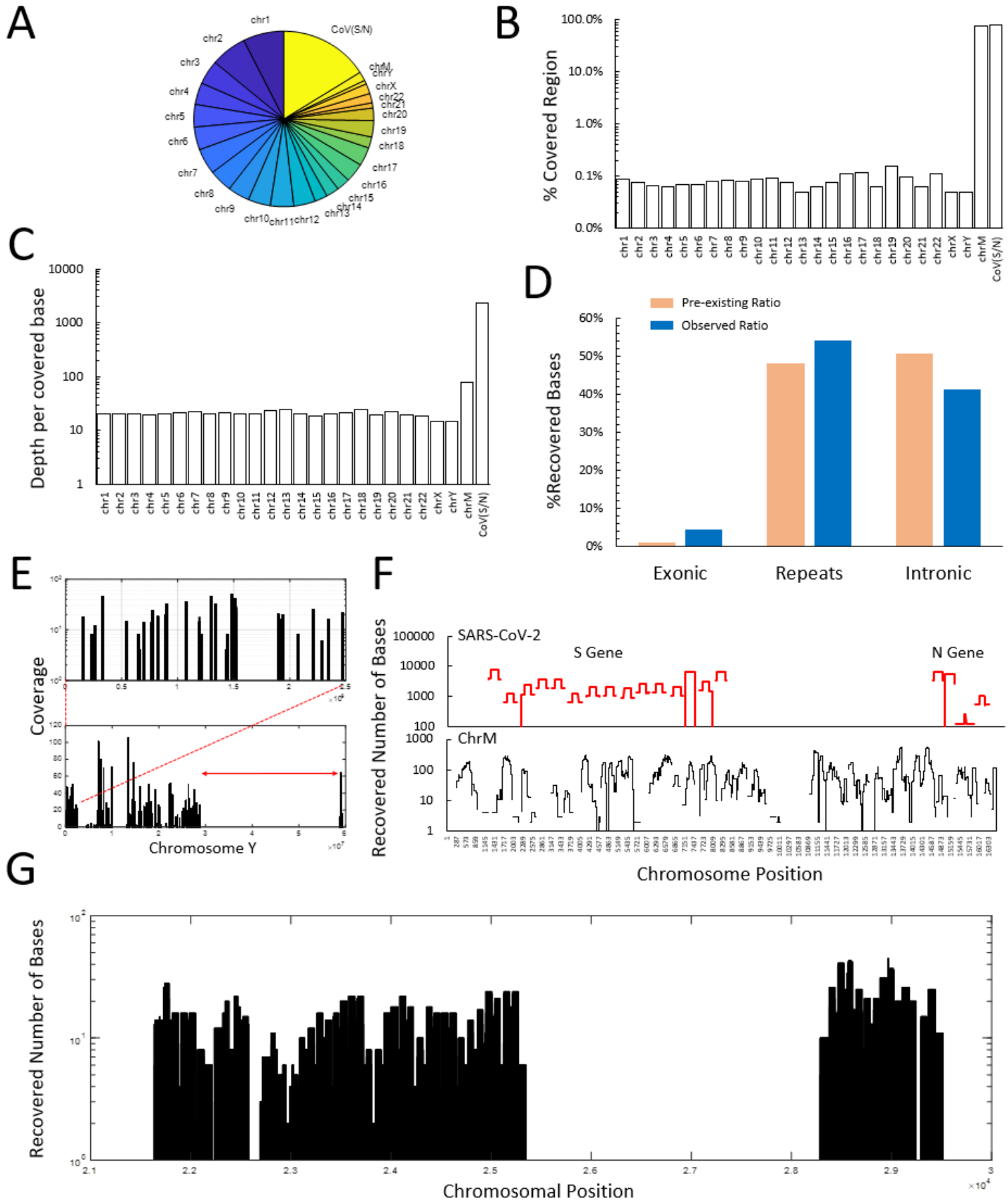
A
chr1
CoV(S/N)
chr2
chr3
chr4
chr5
chr6
chr7
chr8
chr9
chr10
chr11
chr12
chr13
chr14
chr15
chr16
chr17
chr18
chr19
chr20
chr21
chr22
chrX
chrY
chrM
B
% Covered Region
100.0%
10.0%
1.0%
0.1%
0.0%
C
Depth per covered base
10000
1000
100
10
1
D
Pre-existing Ratio
Observed Ratio
%Recovered Bases
60%
50%
40%
30%
20%
10%
0%
Exonic
Repeats
Intronic
E
Coverage
Chromosome Y
F
Recovered Number of Bases
SARS-CoV-2
S Gene
N Gene
ChrM
Chromosome Position
G
Recovered Number of Bases
Chromosomal Position

Figure 4

bioRxiv preprint doi: https://doi.org/10.1101/2020.03.12.988246; this version posted May 18, 2020. The copyright holder for this preprint (which was not certified by peer review) is the author/funder, who has granted bioRxiv a license to display the preprint in perpetuity. It is made available under aCC-BY-NC-ND 4.0 International license.

Supplemental Information

Highly sensitive and full-genome interrogation of SARS-CoV-2 using multiplexed PCR enrichment followed by next-generation sequencing

Chenyu Li[1#], David N. Debruyne[1#], Julia Spencer[1], Vidushi Kapoor[1], Lily Y. Liu[1], Bo Zhou[2], Utsav Pandey[5], Moiz Bootwalla[5], Dejerianne Ostrow[5], Dennis Maglinte[5], David Ruble[5], Alex Ryutov[5], Lishuang Shen[5], Lucie Lee[1], Rounak Feigelman[1], Grayson Burdon[1], Jeffrey Liu[1], Alejandra Oliva[1], Adam Borcherding[3], Hongdong Tan[3,4], Alexander E. Urban[2], Xiaowu Gai[5], Jennifer Dien Bard[5], Guoying Liu[1], Zhitong Liu[1*]

[1] Paragon Genomics Inc., Hayward, CA 94545 USA

[2] Department of Psychiatry and Behavioral Sciences, Department of Genetics, Stanford University, CA 94305 USA

[3] MGI, BGI-Shenzhen, Shenzhen 518083 China

[4] BGI-Shenzhen, Shenzhen 518083 China

[5] Department of Pathology and Laboratory Medicine, Children's Hospital Los Angeles, Los Angeles, CA 90027

[#] These authors contributed equally to the work.

[*] Corresponding author's email: zhitong@paragongenomics.com

bioRxiv preprint doi: https://doi.org/10.1101/2020.03.12.988246; this version posted May 18, 2020. The copyright holder for this preprint (which was not certified by peer review) is the author/funder, who has granted bioRxiv a license to display the preprint in perpetuity. It is made available under aCC-BY-NC-ND 4.0 International license.

Supplemental Fig 1. A mathematical model of RT-PCR.

Supplemental Fig 2. Multiplex PCR efficiency as determined by using CleanPlex® UMI technology by Paragon Genomics.

Supplemental Fig 3. Comparison of LOD between multiplex PCR and regular PCR.

Supplemental Fig 4. Performance statistics of the amplicons retrieved from multiplex PCR method highlighting a 10-fold range read depth.

Supplemental Table 1. Multiplex PCR efficiency as determined by using CleanPlex® UMI technology by Paragon Genomics.

Supplemental Table 2. RT-PCR and sequencing results of SARS-CoV-2 genomes amplified from a cohort of 13 COVID-19 positive patients

Supplemental Table 3. Detected mutations of SARS-CoV-2 in a cohort of 13 COVID-19 positive patients.

Supplemental Table 4. Sequencing results of the multiplex PCR-based metagenomic method using 4,500 copies of plasmids containing SARS-CoV-2 S and N genes spiked in 10ng of human gDNA.

Supplemental Table 5. Performance statistics of the amplicons retrieved from our multiplex PCR method highlighting a 10-fold range read depth.

Supplemental Table 6. Detailed information for the 45 sequenced samples used in this manuscript.

bioRxiv preprint doi: https://doi.org/10.1101/2020.03.12.988246; this version posted May 18, 2020. The copyright holder for this preprint (which was not certified by peer review) is the author/funder, who has granted bioRxiv a license to display the preprint in perpetuity. It is made available under aCC-BY-NC-ND 4.0 International license.

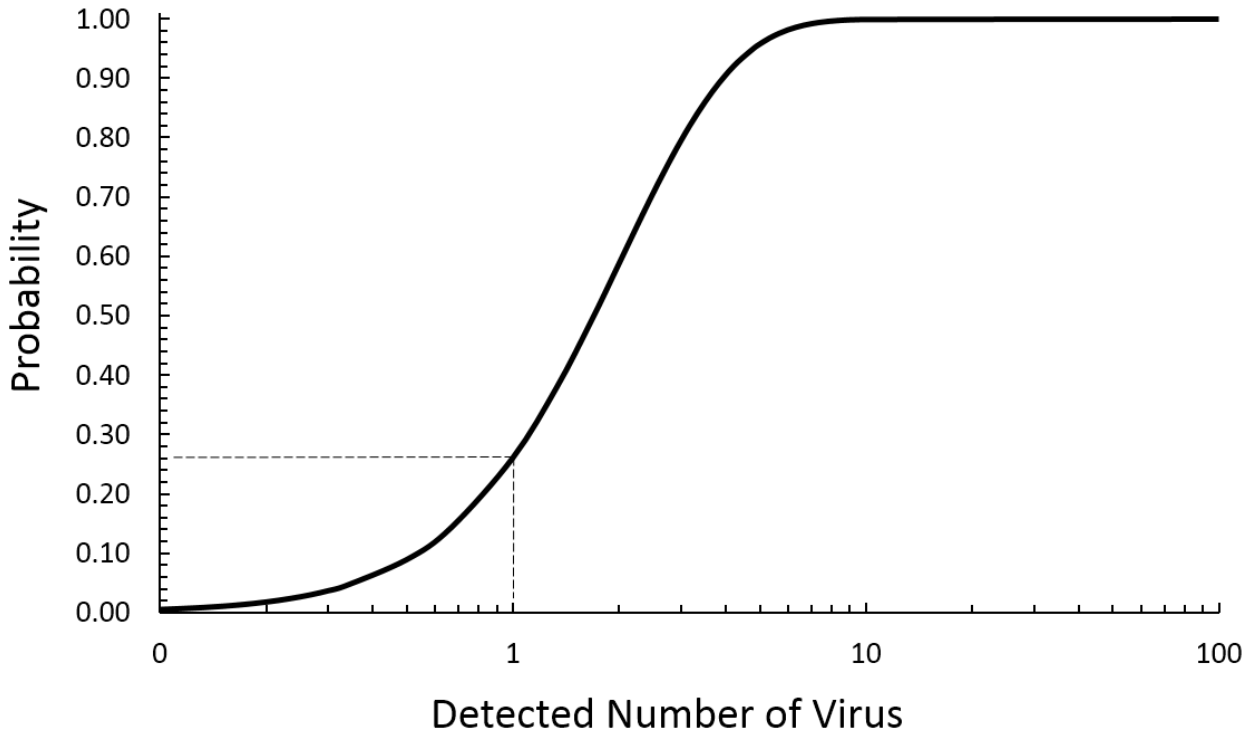

Supplemental Fig 1. A mathematical model of RT-PCR.

The same model was used to estimate the LOD of both RT-PCR and multiplex PCR, through changing the amplicon length and number, the virus genome size, as well as the intended detected copies and PCR efficiency. We found that the probability of detecting 1 copy of SARS-CoV-2 is 26% by using RT-PCR, and the LOD is independent of the length of virus genome.

bioRxiv preprint doi: https://doi.org/10.1101/2020.03.12.988246; this version posted May 18, 2020. The copyright holder for this preprint (which was not certified by peer review) is the author/funder, who has granted bioRxiv a license to display the preprint in perpetuity. It is made available under aCC-BY-NC-ND 4.0 International license.

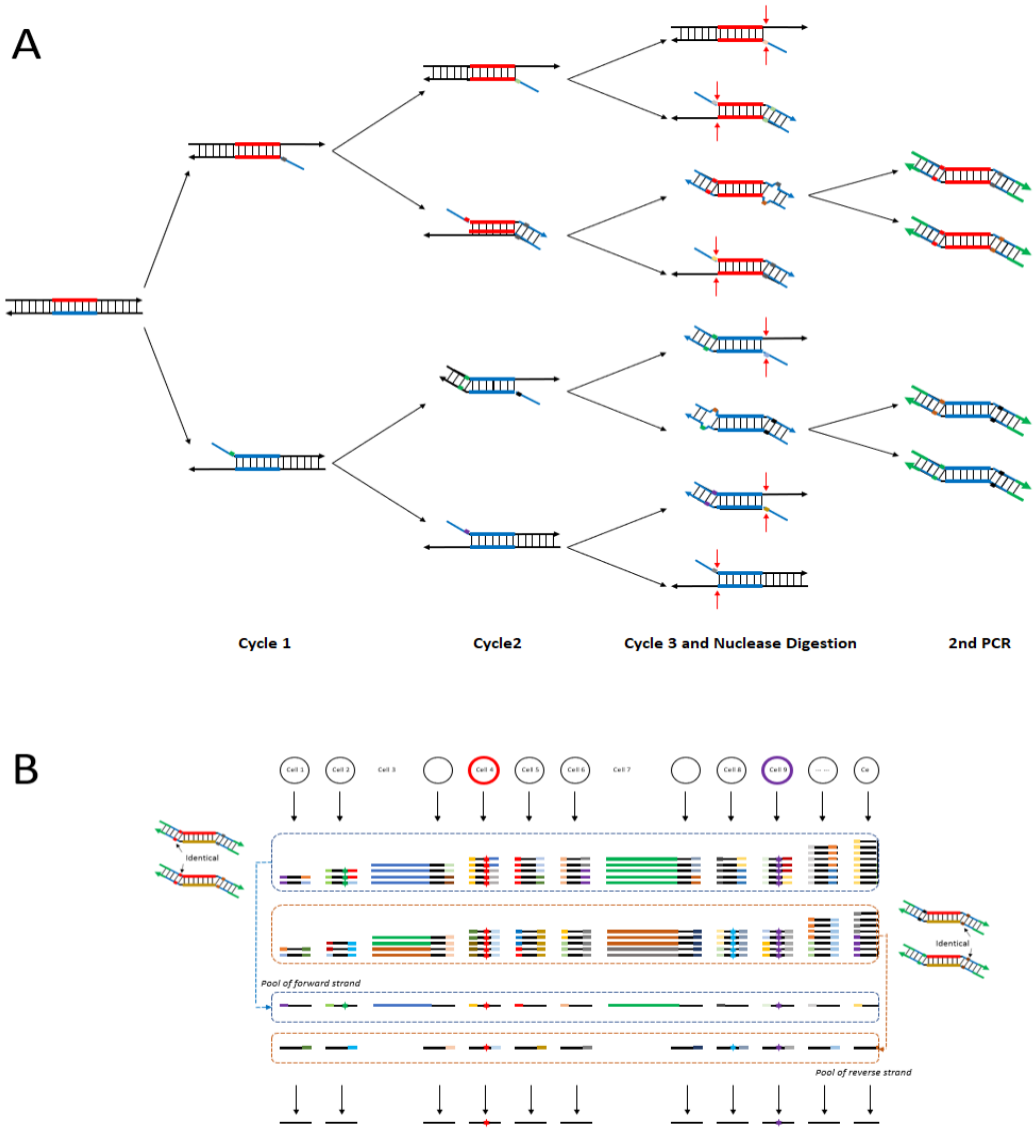

Supplemental Fig 2. Multiplex PCR efficiency as determined by using CleanPlex® UMI technology by Paragon Genomics.

A. The underlying mechanism of CleanPlex® UMI technology by Paragon Genomics, which uses three cycles of multiplex PCR to label targets with UMI. The redundant UMIs generated in the third cycle of PCR are removed through nuclease digestion of the single-stranded regions. The resulting products are further amplified by using a pair of universal primers, while sample indexes and sequencing adapters are introduced. **B.** The UMIs are initially sorted based on the UMI itself, and further on the occurrence of identical UMIs on either the 5′ or 3′ end of amplicons after sequencing, thus allowing the identification of the original template. The position of identical UMIs on either the 5′ or 3′ end of amplicons can further indicate whether the final amplification products are from the pool of the sense or antisense strand of the original templates.

bioRxiv preprint doi: https://doi.org/10.1101/2020.03.12.988246; this version posted May 18, 2020. The copyright holder for this preprint (which was not certified by peer review) is the author/funder, who has granted bioRxiv a license to display the preprint in perpetuity. It is made available under aCC-BY-NC-ND 4.0 International license.

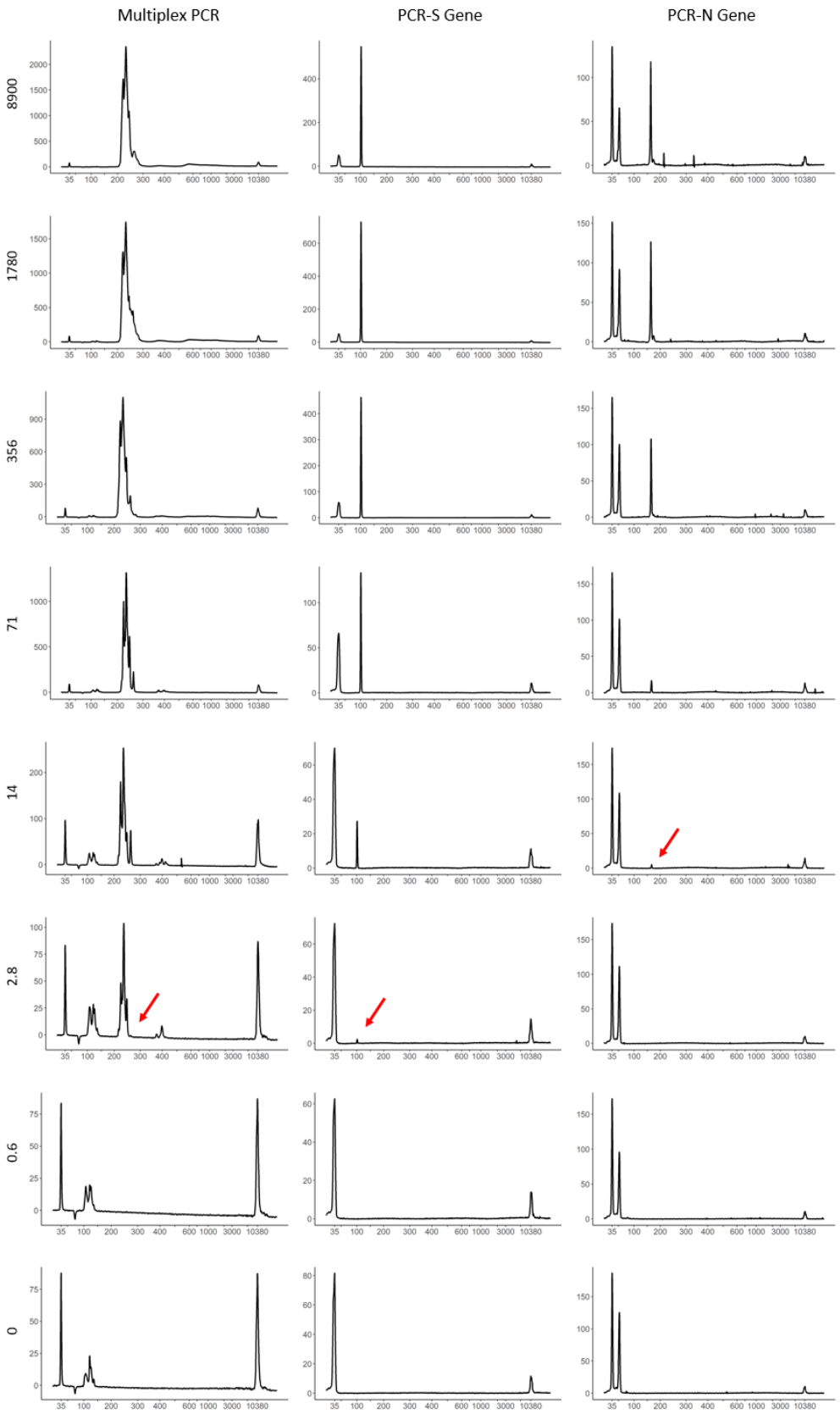

bioRxiv preprint doi: https://doi.org/10.1101/2020.03.12.988246; this version posted May 18, 2020. The copyright holder for this preprint (which was not certified by peer review) is the author/funder, who has granted bioRxiv a license to display the preprint in perpetuity. It is made available under aCC-BY-NC-ND 4.0 International license.

Supplemental Fig 3. Comparison of LOD between multiplex PCR and regular PCR.

A total of 35 cycles was used in multiplex PCR, while 45 cycles were used for regular PCR. The resulting amplification products from multiplex PCR were processed as described in the Materials and Methods. The PCR products were directly resolved using high sensitivity DNA chips on a Bioanalyzer 2100 instrument. X-axis indicates fragment size (bp) and y-axis indicates fluorescence units. The arrows point to the expected specific amplification products. The number of plasmid copies is indicated on the left.

bioRxiv preprint doi: https://doi.org/10.1101/2020.03.12.988246; this version posted May 18, 2020. The copyright holder for this preprint (which was not certified by peer review) is the author/funder, who has granted bioRxiv a license to display the preprint in perpetuity. It is made available under aCC-BY-NC-ND 4.0 International license.

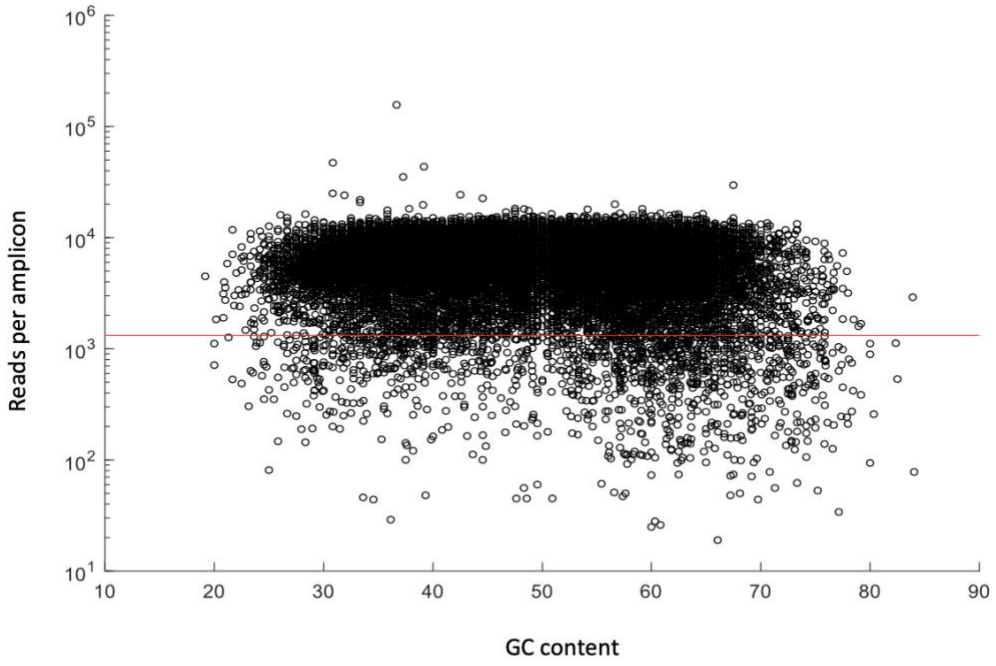

Supplemental Fig 4. Performance statistics of the amplicons retrieved from multiplex PCR method highlighting a 10-fold range read depth.

The number of sequencing reads for a majority of the recovered amplicons (Supplemental Table 5) were within a 10-fold range, representing a uniformity of 92.62 ± 1.96% at 0.2X mean (red line).

bioRxiv preprint doi: https://doi.org/10.1101/2020.03.12.988246; this version posted May 18, 2020. The copyright holder for this preprint (which was not certified by peer review) is the author/funder, who has granted bioRxiv a license to display the preprint in perpetuity. It is made available under aCC-BY-NC-ND 4.0 International license.

Supplemental Table 1. Multiplex PCR efficiency as determined by using CleanPlex® UMI technology by Paragon Genomics.

A 53-amplicon panel was amplified with 20 to 80 ng of gDNA (NA12878) by using CleanPlex® UMI technology by Paragon Genomics, the mechanism of which is depicted in Supplemental Fig 2. The efficiency of multiplex PCR was found to be 26%, calculated from the recovered numbers of UMI clusters that contained >= 3 members (UMI (>=3)).

DNA ng	Uniformity 0.2X Mean (%)	Total UMI	UMI (=1)	UMI (>=3)	UMI (>=5)	Raw Reads	Mapped Reads	On-target Reads	Total UMI Reads	UMI (>=3) Reads	Haploid Genomes	UMI (>=3) eff.	%UMI (>=3)
20	98.1%	530874	165687	351904	322511	5508532	4321171	4014880	3551662	3359409	1660	25.2%	66.3%
20	100.0%	448374	96774	327229	252561	3430557	2727335	2557727	2351544	2206028	1544	23.4%	73.0%
20	98.1%	613434	236067	364231	353500	8939089	7048505	6572606	5903206	5640867	1718	26.0%	59.4%
30	96.2%	982983	401164	560890	527993	9037026	7765886	7485868	6561378	6118356	2646	26.7%	57.1%
30	98.1%	812441	236456	553325	496326	7485107	6254270	5877149	5189318	4907542	2610	26.4%	68.1%
30	98.1%	722872	128591	580862	556866	9854077	7727106	7714642	7487927	7332504	2740	27.7%	80.4%
30	98.1%	709433	105870	587582	549015	8472590	6610966	6599497	6411865	6274035	2772	28.0%	82.8%
30	98.1%	693711	141968	507126	371323	4700397	3975741	3768653	3458895	3227693	2392	24.2%	73.1%
30	98.1%	929401	333715	575663	557579	12185504	10230011	9645802	8648217	8274456	2715	27.4%	61.9%
50	96.2%	1521124	504587	970308	841045	12240066	10145239	9795805	8610343	8013298	4577	27.7%	63.8%
80	96.2%	2055833	623322	1344679	1078860	14037982	12323533	11897105	10482966	9683980	6343	24.0%	65.4%
Avg.												26.1%	68.3%
STDEV												1.7%	8.2%

bioRxiv preprint doi: https://doi.org/10.1101/2020.03.12.988246; this version posted May 18, 2020. The copyright holder for this preprint (which was not certified by peer review) is the author/funder, who has granted bioRxiv a license to display the preprint in perpetuity. It is made available under aCC-BY-NC-ND 4.0 International license.

Supplemental Table 2. RT-PCR and sequencing results of SARS-CoV-2 genomes amplified from a cohort of 13 COVID-19 positive patients

ID	Copy Number	Uniformity 0.2X Mean (%)	Mapping Rate (%)	On-Target Rate (%)	Total Reads	Mapped Reads	On-Target Reads	Primer Dimer Reads	Primer Dimer Rate (%)	Average On-Target Reads per Amplicon
CHLA9	8	65.31	99.81	89.26	1110606	1108547	989515	493	0.05	2884
CHLA10	22	87.46	84.51	93.14	845394	714470	665443	20129	3.02	1940
CHLA11	89	71.72	99.90	96.47	1740180	1738420	1677034	869	0.05	4889
CHLA1	319	97.38	98.03	99.21	802986	787187	780950	1894	0.24	2276
CHLA2	2310	96.21	95.92	99.13	1420132	1362254	1350437	7013	0.52	3937
CHLA3	3460	90.67	96.8	98.42	665536	644217	634048	3132	0.49	1848
CHLA12	4999	63.85	99.73	93.83	1551346	1547177	1451691	8812	0.61	4232
CHLA4	10367	95.04	99.83	98.08	2620898	2616444	2566262	1585	0.06	7481
CHLA5	37758	95.04	99.32	99.20	2282126	2266649	2248408	1235	0.05	6555
CHLA13	52735	95.92	99.94	98.96	2480938	2479370	2453510	186	0.01	7153
CHLA6	156882	93.59	99.77	99.43	1890384	1885967	1875238	462	0.02	5467
CHLA7	233844	94.75	99.79	99.00	2252828	2248089	2225503	308	0.01	6488
CHLA8	675855	95.63	99.96	97.63	3594226	3592758	3507470	49	0.00	10225
MN908947.3	500000	90.96	99.71	98.64	2656772	2649047	2613012	271	0.01	7618

bioRxiv preprint doi: https://doi.org/10.1101/2020.03.12.988246; this version posted May 18, 2020. The copyright holder for this preprint (which was not certified by peer review) is the author/funder, who has granted bioRxiv a license to display the preprint in perpetuity. It is made available under aCC-BY-NC-ND 4.0 International license.

Supplemental Table 3. Detected SARS-CoV-2 mutations in a cohort of 13 COVID-19 positive patients.

Twist SARS-CoV-2 control		CHLA1_319 copies		CHLA2_2310 copies		CHLA3_3460 copies		CHLA4_10367 copies (Batch1_S2)		CHLA5_S5_37758 copies		CHLA6_156882 copies		CHLA7_233844 copies		CHLA8_675885 copies (Batch1_S5)		CHLA9_8 (Batch1_S1)		CHLA10_S4_22		CHLA11_89 (Batch1_S6)		CHLA12_4999 (Batch1_S3)		CHLA13_52735 copies (Batch1_S4)	
Mutation	Allele Frequency	Mutation	Allele Frequency	Mutation	Allele Frequency	Mutation	Allele Frequency	Mutation	Allele Frequency	Mutation	Allele Frequency	Mutation	Allele Frequency	Mutation	Allele Frequency	Mutation	Allele Frequency	Mutation	Allele Frequency	Mutation	Allele Frequency	Mutation	Allele Frequency	Mutation	Allele Frequency	Mutation	Allele Frequency
T19065C	99.4%	C241T	93.0%	C241T	99.7%	C241T	98.7%	C241T	98.4%	C241T	99.4%	C241T	99.5%	C241T	99.5%	C241T	99.4%	C241T	100.0%	C241T	83.2%	C241T	41.0%	C241T	99.4%	T490A	99.0%
T22303G	99.0%	C379A	93.7%	C379A	99.7%	T833C	24.3%	C379A	96.4%	C379A	99.5%	C379A	99.3%	C379A	99.5%	T833C	99.3%	G247A	35.9%	T833C	58.9%	C379A	28.1%	C379A	82.7%	C3177T	98.2%
G26144T	99.3%	C897T	94.2%	C897T	99.2%	C3037T	99.0%	C1059T	99.5%	C897T	99.4%	C1059T	99.4%	C1059T	99.7%	C1059T	99.7%	C379A	54.5%	C1059T	84.9%	T833C	41.7%	C3037T	47.6%	C6040T	98.8%
Del29749(10	99.5%	C1059T	91.8%	C1059T	99.4%	C14408T	97.1%	C3037T	60.6%	C1059T	99.4%	A1486C	99.7%	C3037T	99.7%	C3037T	99.3%	C1059T	100.0%	TA2904T	22.3%	C3037T	57.1%	C5547T	55.3%	C8782T	98.9%
		C3037T	96.5%	C3037T	99.6%	A23403G	94.5%	C14408T	66.6%	C3037T	99.3%	C3037T	99.5%	C4002T	99.7%	C14408T	99.5%	C3037T	46.4%	C3037T	99.8%	C14408T	64.4%	T7430C	20.5%	G12478A	99.6%
		C14408T	98.2%	C14408T	99.4%	A26530G	95.9%	A23403G	83.4%	C14408T	99.5%	C3736T	99.5%	C14408T	99.5%	C20099T	73.7%	C8782T	36.7%	Del4531(16)	75.9%	C20099T	55.0%	Del8750(25)	31.2%	T18736C	98.8%
		A23403G	92.9%	A23403G	98.6%			G25563T	99.8%	A23403G	98.9%	A5010T	99.7%	A23403G	98.8%	A23403G	98.6%	C14408T	39.8%	T5479C	25.9%	A23403G	76.4%	T11408C	97.8%	C24034T	98.6%
		G25563T	89.4%	G25563T	99.4%			T26729C	29.2%	G25563T	99.5%	G11893T	99.3%	G25563T	99.5%	G25563T	99.4%	C20099T	26.0%	C7329T	28.0%	G25563T	38.8%	C14408T	28.7%	T26729C	93.5%
		Del29749(10	83.3%							C25669T	31.7%	C14408T	99.2%			C26912T	99.6%	A23403G	56.5%	C9661T	28.2%	T26729C	31.7%	C20099T	21.5%	G28077C	97.2%
												G16707T	99.3%			C27964T	99.5%	G25563T	100.0%	C14408T	78.3%	C26912T	41.6%	T20612C	40.5%	T28144C	96.4%
												A23403G	98.5%					T26729C	36.4%	T18736C	23.1%	C27964T	65.9%	C22350T	32.8%	C28896G	94.6%
												A24922G	99.2%					C26912T	52.8%	C20099T	30.4%			G25563T	100.0%	A29700G	42.5%
												G25563T	99.7%					C27964T	39.1%	A21617G	27.9%			Del26133(30)	30.9%		
																				G22026T	28.1%			G26634A	21.6%		
																				A23403G	93.2%			T26729C	50.8%		
																				G25290T	37.3%			C26912T	33.2%		
																				G25563T	97.9%						

bioRxiv preprint doi: https://doi.org/10.1101/2020.03.12.988246; this version posted May 18, 2020. The copyright holder for this preprint (which was not certified by peer review) is the author/funder, who has granted bioRxiv a license to display the preprint in perpetuity. It is made available under aCC-BY-NC-ND 4.0 International license.

Supplemental Table 4. Sequencing results of the multiplex PCR-based metagenomic method using 4,500 copies of plasmids containing SARS-CoV-2 S and N genes spiked in 10ng of human gDNA.

	Covered Region (Bases)	Recovered Bases	Existing Bases	%Base Covered	Depth per Base	%Base Recovered	# Continuous Regions	Max Length
chr1	217690	4374253	249250621	0.087%	20	7.36%	1871	635
chr2	189593	3878281	243199373	0.078%	20	6.52%	1677	400
chr3	130594	2644455	198022430	0.066%	20	4.45%	1195	498
chr4	121131	2380497	191154276	0.063%	20	4.00%	1084	521
chr5	124355	2477809	180915260	0.069%	20	4.17%	1144	298
chr6	117578	2507731	171115067	0.069%	21	4.22%	1039	331
chr7	128702	2811905	159138663	0.081%	22	4.73%	1114	853
chr8	120983	2501918	146364022	0.083%	21	4.21%	1046	615
chr9	110739	2331049	141213431	0.078%	21	3.92%	959	316
chr10	117000	2391950	135534747	0.086%	20	4.02%	1007	570
chr11	123298	2491047	135006516	0.091%	20	4.19%	1055	769
chr12	101440	2318400	133851895	0.076%	23	3.90%	899	302
chr13	56253	1362272	115169878	0.049%	24	2.29%	504	484
chr14	67012	1393000	107349540	0.062%	21	2.34%	595	317
chr15	78397	1437683	102531392	0.076%	18	2.42%	668	312
chr16	99946	2074762	90354753	0.111%	21	3.49%	829	418
chr17	95737	2028045	81195210	0.118%	21	3.41%	793	315
chr18	50052	1211867	78077248	0.064%	24	2.04%	431	481
chr19	91863	1783580	59128983	0.155%	19	3.00%	774	388
chr20	61046	1371117	63025520	0.097%	22	2.31%	525	431
chr21	29838	577980	48129895	0.062%	19	0.97%	266	403
chr22	56658	1032340	51304566	0.110%	18	1.74%	447	303
chrX	75130	1097325	155270560	0.048%	15	1.85%	736	294
chrY	28987	417843	59373566	0.049%	14	0.70%	259	289
chrM	12851	992192	16571	77.55%	77	1.67%	32	1874
CoV(S/N)	4075	9558337	5082	80.18%	2346	16.08%	32	273

bioRxiv preprint doi: https://doi.org/10.1101/2020.03.12.988246; this version posted May 18, 2020. The copyright holder for this preprint (which was not certified by peer review) is the author/funder, who has granted bioRxiv a license to display the preprint in perpetuity. It is made available under aCC-BY-NC-ND 4.0 International license.

Supplemental Table 5. Performance statistics of the amplicons retrieved from our multiplex PCR method highlighting a 10-fold range of read depth.

To simulate multiplex PCR with random hexamers as primers, we used a panel of 27,296 pairs of primers to perform multiplex PCR. These primers were divided into 2 overlapping primer pools, and amplification was initially performed in two separate reactions. The number of sequencing reads for a majority of the recovered amplicons were within a 10-fold range, representing a uniformity of 92.62 ± 1.96% at 0.2X mean.

Sample Number	Uniformity 0.2X Mean (%)	Mapping Rate (%)	On-Target Rate (%)	Total Reads	Mapped Reads	On-Target Reads	Primer Dimer Reads	Primer Dimer Rate (%)	Average On-Target Reads per Amplicon
1	93.6%	94.0%	96.2%	269435076	253341610	243602321	3326193	1.31%	8924
2	92.7%	97.3%	95.9%	272733262	265270282	254306010	1920151	0.72%	9316
3	92.8%	96.6%	95.8%	188776124	182357219	174778001	1492049	0.82%	6403
4	93.1%	97.2%	95.7%	265645114	258182429	247093224	1879080	0.73%	9052
5	92.6%	97.1%	95.5%	232875020	226046731	215875589	1535441	0.68%	7908
6	93.5%	97.1%	96.2%	192403072	186821637	179683779	1266338	0.68%	6582
7	91.3%	96.5%	96.5%	181465458	175141658	168975648	1423714	0.81%	6190
8	88.1%	96.7%	96.6%	191995346	185607975	179350573	1390209	0.75%	6570
9	95.0%	97.2%	95.3%	197356014	191797447	182683756	1056748	0.55%	6692
10	95.0%	96.5%	95.7%	201474266	194391114	185997107	1317629	0.68%	6814
11	95.0%	96.7%	96.5%	193125370	186751406	180154727	1036439	0.55%	6600
12	88.2%	95.5%	97.0%	199616350	190581763	184843808	1908098	1.00%	6771
13	92.0%	93.3%	96.4%	272873692	254679030	245480306	3824568	1.50%	8993
14	94.0%	93.6%	95.9%	297541418	278622642	267164257	4259698	1.53%	9787
15	91.2%	91.7%	96.3%	323595774	296801010	285698174	5184019	1.75%	10466
16	91.4%	93.9%	96.3%	248888684	233638153	224968924	5337352	2.28%	8241
17	91.5%	97.3%	96.8%	206702726	201183261	194776826	2063586	1.03%	7135
18	91.5%	98.2%	96.9%	178948198	175675252	170297061	1083447	0.62%	6238
19	90.2%	99.0%	97.1%	206684484	204582941	198563161	708813	0.35%	7274
20	91.1%	87.3%	95.0%	397262166	346621107	329334881	17048174	4.92%	12065
21	94.5%	95.5%	96.1%	215357334	205717503	197695646	2174832	1.06%	7242
22	94.1%	99.1%	95.9%	166942258	165384936	158665846	425846	0.26%	5812
23	94.2%	98.7%	96.0%	198067370	195451983	187701462	631609	0.32%	6876
24	94.2%	98.6%	96.1%	169536088	167192888	160657429	514940	0.31%	5885
25	94.8%	91.4%	94.9%	356335780	325681114	308973305	8034601	2.47%	11319
Avg.	92.6%	95.8%	96.1%					1.11%	7806
STDEV	1.96%	2.77%	0.58%					0.98%	1739
CV	2.12%	2.89%	0.60%					88.6%	22.3%

bioRxiv preprint doi: https://doi.org/10.1101/2020.03.12.988246; this version posted May 18, 2020. The copyright holder for this preprint (which was not certified by peer review) is the author/funder, who has granted bioRxiv a license to display the preprint in perpetuity. It is made available under aCC-BY-NC-ND 4.0 International license.

Supplemental Table 6. Detailed information for the 45 sequenced samples used in this manuscript.

NCBI's Sequence Read Archive (SRA) Sample ID and accession numbers for all 45 sequenced samples, along with sequencing details, sample description and the figure in which each sample's data has been used is listed in this table. These fastq files are available for downloading at https://www.ncbi.nlm.nih.gov/Traces/study/?acc=PRJNA614546

Sample	File Name	Figure	Content	Accession	Isolation Source
10	ILLUMINA (Illumina iSeq 100) run: 193,681 spots, 58.5M bases, 15.6Mb downloads	Figure 2D	2.8 copies_1	SRX7976138	Plasmid
9	ILLUMINA (Illumina iSeq 100) run: 222,876 spots, 67.3M bases, 17.9Mb downloads	Figure 2D	2.8 copies_2	SRX7976139	Plasmid
8	ILLUMINA (Illumina iSeq 100) run: 18,392 spots, 5.6M bases, 1.7Mb downloads	Figure 2D	2.8 copies_3	SRX7976140	Plasmid
7	ILLUMINA (Illumina iSeq 100) run: 900,360 spots, 271.9M bases, 72.1Mb downloads	Figure 2D	1.4 copies_1	SRX7976141	Plasmid
6	ILLUMINA (Illumina iSeq 100) run: 144,240 spots, 43.6M bases, 11.8Mb downloads	Figure 2D	1.4 copies_2	SRX7976142	Plasmid
5	ILLUMINA (Illumina iSeq 100) run: 977,584 spots, 295.2M bases, 83.5Mb downloads	Figure 2D	1.4 copies_3	SRX7976143	Plasmid
4	ILLUMINA (Illumina iSeq 100) run: 457,181 spots, 138.1M bases, 46.9Mb downloads	Figure 3	Metagenomics	SRX7976144	Plasmid
3	ILLUMINA (Illumina iSeq 100) run: 517,641 spots, 156.3M bases, 45Mb downloads	Figure 4	Meta_20 dilution	SRX7976145	Plasmid
2	ILLUMINA (Illumina iSeq 100) run: 613,188 spots, 185.2M bases, 53.5Mb downloads	Figure 4	Meta_4 dilution	SRX7976146	Plasmid
1	ILLUMINA (Illumina iSeq 100) run: 565,052 spots, 170.6M bases, 49.2Mb downloads	Figure 4	Meta_0.8 dilution	SRX7976147	Plasmid
31	BGISEQ (BGISEQ-500) run: 21M spots, 2.1G bases, 1Gb downloads	Figure 2E	500 dilution_1	SRX7990909	Plasmid
30	BGISEQ (BGISEQ-500) run: 21.5M spots, 2.1G bases, 1Gb downloads	Figure 2E	100 dilution_1	SRX7990910	Plasmid
17	BGISEQ (BGISEQ-500) run: 16.5M spots, 1.7G bases, 817.7Mb downloads	Figure 2E	20 dilution_1	SRX7990923	Plasmid
16	BGISEQ (BGISEQ-500) run: 18.4M spots, 1.8G bases, 917.7Mb downloads	Figure 2E	4 dilution_1	SRX7990924	Plasmid
15	BGISEQ (BGISEQ-500) run: 24.7M spots, 2.5G bases, 1.2Gb downloads	Figure 2E	0.8 dilution_1	SRX7990925	Plasmid
14	BGISEQ (BGISEQ-500) run: 9.2M spots, 924.4M bases, 420.4Mb downloads	Figure 2E	0.16 dilution_1	SRX7990926	Plasmid
13	BGISEQ (BGISEQ-500) run: 12.3M spots, 1.2G bases, 507.6Mb downloads	Figure 2E	0 dilution_1	SRX7990927	Plasmid
12	BGISEQ (BGISEQ-500) run: 15.8M spots, 1.6G bases, 794.3Mb downloads	Figure 2E	500 dilution_2	SRX7990928	Plasmid
11	BGISEQ (BGISEQ-500) run: 16.3M spots, 1.6G bases, 818.2Mb downloads	Figure 2E	100 dilution_2	SRX7990929	Plasmid
29	BGISEQ (BGISEQ-500) run: 23.8M spots, 2.4G bases, 1.2Gb downloads	Figure 2E	20 dilution_2	SRX7990911	Plasmid
28	BGISEQ (BGISEQ-500) run: 6.9M spots, 693.4M bases, 343.4Mb downloads	Figure 2E	4 dilution_2	SRX7990912	Plasmid
27	BGISEQ (BGISEQ-500) run: 3M spots, 300.2M bases, 146.1Mb downloads	Figure 2E	0.8 dilution_2	SRX7990913	Plasmid
26	BGISEQ (BGISEQ-500) run: 4.6M spots, 455M bases, 225.3Mb downloads	Figure 2E	0.16 dilution_2	SRX7990914	Plasmid
25	BGISEQ (BGISEQ-500) run: 2.1M spots, 211.3M bases, 98.1Mb downloads	Figure 2E	0 dilution_2	SRX7990915	Plasmid
24	BGISEQ (BGISEQ-500) run: 28.7M spots, 2.9G bases, 1.4Gb downloads	Figure 2E	500 dilution_3	SRX7990916	Plasmid
23	BGISEQ (BGISEQ-500) run: 19.3M spots, 1.9G bases, 948.2Mb downloads	Figure 2E	100 dilution_3	SRX7990917	Plasmid
22	BGISEQ (BGISEQ-500) run: 39M spots, 3.9G bases, 1.8Gb downloads	Figure 2E	20 dilution_3	SRX7990918	Plasmid
21	BGISEQ (BGISEQ-500) run: 42.5M spots, 4.3G bases, 2Gb downloads	Figure 2E	4 dilution_3	SRX7990919	Plasmid
20	BGISEQ (BGISEQ-500) run: 46.8M spots, 4.7G bases, 2.1Gb downloads	Figure 2E	0.8 dilution_3	SRX7990920	Plasmid
19	BGISEQ (BGISEQ-500) run: 26.2M spots, 2.6G bases, 1Gb downloads	Figure 2E	0.16 dilution_3	SRX7990921	Plasmid
18	BGISEQ (BGISEQ-500) run: 35M spots, 3.5G bases, 1.3Gb downloads	Figure 2E	0 dilution_3	SRX7990922	Plasmid
32	1 ILLUMINA (Illumina MiSeq) run: 555,303 spots, 164.6M bases, 83Mb downloads	Figure 3	CHLA2	SRX8264270	nasal swab
33	1 ILLUMINA (Illumina MiSeq) run: 1.3M spots, 384.9M bases, 201.7Mb downloads	Figure 3	CHLA5	SRX8264269	nasal swab
34	1 ILLUMINA (Illumina MiSeq) run: 775,686 spots, 226.8M bases, 114.3Mb downloads	Figure 3	CHLA3	SRX8264268	nasal swab
35	1 ILLUMINA (Illumina MiSeq) run: 1.2M spots, 364.9M bases, 188.1Mb downloads	Figure 3	CHLA7	SRX8264267	nasal swab
36	1 ILLUMINA (Illumina MiSeq) run: 1.8M spots, 525.7M bases, 266.9Mb downloads	Figure 3	CHLA11	SRX8264266	nasal swab
37	1 ILLUMINA (Illumina MiSeq) run: 870,090 spots, 256.9M bases, 130.8Mb downloads	Figure 3	CHLA8	SRX8264265	nasal swab
38	1 ILLUMINA (Illumina MiSeq) run: 1.1M spots, 340.2M bases, 176.6Mb downloads	Figure 3	CHLA13	SRX8264264	nasal swab
39	1 ILLUMINA (Illumina MiSeq) run: 332,823 spots, 100.5M bases, 51.2Mb downloads	Figure 3	CHLA12	SRX8264263	nasal swab
40	1 ILLUMINA (Illumina MiSeq) run: 1.1M spots, 344.6M bases, 173.4Mb downloads	Figure 3	MN908947.3 (Twist SARS-CoV-2 RNA)	SRX8264262	not applicable
41	1 ILLUMINA (Illumina MiSeq) run: 710,098 spots, 214.4M bases, 110.6Mb downloads	Figure 3	CHLA10	SRX8264261	nasal swab
42	1 ILLUMINA (Illumina MiSeq) run: 401,508 spots, 121.3M bases, 63Mb downloads	Figure 3	CHLA6	SRX8264260	nasal swab
43	1 ILLUMINA (Illumina MiSeq) run: 945,198 spots, 285.4M bases, 144.1Mb downloads	Figure 3	CHLA1	SRX8264259	nasal swab
44	1 ILLUMINA (Illumina MiSeq) run: 422,863 spots, 127.7M bases, 70Mb downloads	Figure 3	CHLA4	SRX8264258	nasal swab
45	1 ILLUMINA (Illumina MiSeq) run: 1.3M spots, 401.2M bases, 203.1Mb downloads	Figure 3	CHLA9	SRX8264257	nasal swab